UNIVERSITY OF CALIFORNIA
RIVERSIDE

Radiative Neutrino Mass, Dark Matter, Flavor Symmetry, and Collider Signatures

A Dissertation submitted in partial satisfaction
of the requirements for the degree of

Doctor of Philosophy

in

Physics

by

Alexander Natale

August 2015

Dissertation Committee:

Dr. Ernest Ma, Chairperson
Dr. Jose Wudka
Dr. Hai-Bo Yu

The Dissertation of Alexander Natale is approved:

Committee Chairperson

University of California, Riverside

Acknowledgments

I am grateful to my advisor, Dr. Ernest Ma whose guidance, knowledge, and patience over the years have made this thesis possible. I am also very grateful to my committee members Dr. Jose Wudka and Dr. Hai-Bo Yu for their advice and support, and giving aid ceaselessly anytime I needed it.

I would also like to thank Dr. Subhaditya Bhattacharya, Dr. Daniel Wegman, and Dr. Ahmed Rashid for all the knowledge they have passed on during my PhD. Additionally, I would like to thank Mohammadreza Zakeri and Sean Fraser, with whom I have had very enlightening discussions while writing this thesis.

I wish to express my love and eternal thanks to my wife Kayleigh, Mom, Dad, Sarah, Jodey, Michael, and Hope. Without the support they have given me, I would not have reached this point. I extend a special thanks to my friends Mike Beaumier and Jackie Hubbard, whose support and friendship are invaluable.

The work that appears in this thesis is based on previously published work from Refs. [1–6]. I thank and acknowledge the contribution of my co-authors to these published works.

This thesis is dedicated to my loving wife, Kayleigh Anderson-Natale.

ABSTRACT OF THE DISSERTATION

Radiative Neutrino Mass, Dark Matter, Flavor Symmetry, and Collider Signatures

by

Alexander Natale

Doctor of Philosophy, Graduate Program in Physics
University of California, Riverside, August 2015
Dr. Ernest Ma, Chairperson

The current understanding of particle physics is condensed into a single model known as the Standard Model, which has had remarkable success at describing the observed interactions of fundamental particles. Since the discovery of the 125 GeV Higgs boson at the Large Hadron Collider in 2012, the Standard Model appears to be complete. However, the astrophysical observations of dark matter and the existence of neutrino mass are strongly compelling reasons to think there is physics beyond the Standard Model. In 2006 a proposal was made that these two phenomena are actually connected, and that the existence of neutrino mass is tied to neutrino interactions with dark matter and other components of the dark sector. This original proposal — known as the scotogenic model — has been extended to include self-interacting dark matter, the generation of lepton and quark mass, various flavor symmetries, and has also been studied with alternative particle content. In this thesis, several scotogenic models of neutrino oscillation with various symmetries are studied, and the predictions for future neutrino oscillation experiments along with potentially interesting signatures at the 13 TeV LHC run are discussed.

Contents

List of Figures

List of Tables

Part I

Introduction and Background

Chapter 1

Introduction

This Thesis is divided into three parts: **(I)** a description of relevant background, descriptions of crucial theory, and a discussion of the scotogenic model of neutrino mass and basic extensions; **(II)** a detailed description and discussion of specific models, results, and methods; **(III)** conclusions and discussion, the bibliography, and the appendices. A working knowledge of quantum field theory, the Standard Model (SM), and particle physics along with basic familiarity with supersymmetry (SUSY) and relevant experiments such as the Large Hadron Collider has been assumed.

Part **I** is comprised of two chapters. Chapter 2 contains a brief summary of the Standard Model (SM), a summary of dark matter (DM) physics, and a description of neutrino mass and oscillation. The discussion on neutrino mass and oscillation is further divided into four parts. Section 2.3.1 contains a discussion of neutrino mass, oscillation, the experimental results and unresolved questions. Section 2.3.2 is a discussion of the motivations and a brief discussion of the application of flavor symmetries to neutrino oscillation. Section 2.3.3 is an introduction of the scotogenic model of neutrino mass which is the theoretical framework that acts as the basis of the bulk of the work contained in this thesis. And finally, Section 2.3.4 is the last section is a discussion of extensions of the minimal scotogenic model.

Part **II** is divided into two chapters. Chapter 1 is focused on the analysis of specific

models of particle physics with an emphasis on explaining various patterns of neutrino oscillation. Chapter 2 is focused on the analysis of specific models with an emphasis on making concrete predictions for the Large Hadron Collider (LHC), located at the border of Switzerland and France.

And finally, part **III** contains the summary and discussion ,the bibliography, and the appendices that contain a brief review of relevant group theory and non-Abelian discrete groups, the details of the minimal scotogenic loop calculation, and the details for the inverse scotogenic loop calculation respectively.

Chapter 2

Background

2.1 Standard Model

The Standard Model (SM) of particle physics is remarkably successful at describing fundamental physical interactions of the known elementary particles. As is well known, the SM describes physical interactions using a Langrangian density that has a local gauge invariance under $SU(3)_C \times SU(2)_L \times U(1)_Y$, which describes the interactions of fermions (the quarks and leptons) and a single scalar the Higgs boson via the force carrying gauge bosons (the photon, gluons, and the W and Z bosons). The Higgs mechanism leads to the spontaneous symmetry breaking of $SU(2)_L$, and explains the origin of quark and charged lepton masses, as well as the masses for the W and Z bosons. A fundamental scalar consistent with the properties of the SM Higgs boson has recently been observed at the Large Hadron Collider (LHC) [7,8], and so in many ways the SM is a complete, fully renormalizable quantum field theory of fundamental particle physics [9, 10].

Despite its successes, there are challenges and unanswered questions that remain in the minimal SM. The search for unambiguous evidence of physics beyond the SM is well underway at the LHC, however nothing beyond a SM-like Higgs boson with a mass of 125 GeV [7, 8] has been found. Despite the lack of evidence for new physics in particle colliders, there are large bodies of experimental evidence that imply the existence of physics

that isn't explained by the minimal SM. In particular neutrino mass and dark matter (DM) provide two major examples where observations cannot be accommodated by the minimal Standard Model. The experimental evidence for neutrino oscillation, and thus the existence of nonzero neutrino mass, is overwhelming [11–20]. Additionally, many sources of astrophysical evidence convincingly demonstrate the existence of dark matter [21–31]. It is crucial for any model of particle physics beyond the SM to provide explanations for both of these phenomenon. A large motivation for the work presented in this thesis is the suggestion that the phenomenon of dark matter and neutrino mass are, in fact, deeply related [32]. Dubbed the scotogenic model, from the Greek word 'scotos' which means darkness, this 2006 proposal explains the smallness of neutrino mass via a loop-generated mass where DM plays a central role in completing the loop. This original motivation has recently been extended to include a scotogenic generation of the lighter lepton and quark masses [33], extended with discrete flavor symmetries (for an example see Ref. [1]), and has also been studied with an extended gauge group as discussed in Ref. [34]. Such models provide very interesting phenomenology in the so-called dark sector as well as providing potentially interesting collider results.

2.2 Dark Matter

The evidence for Dark Matter comes from a variety of sources which includes rotation curves of spiral galaxies [23–25], strong and weak gravitational lensing [26–29], data from the cosmic microwave background (CMB) [21, 22], data from dwarf spheroidal galaxies [30, 31] and from many other sources of evidence. From these observations, a few key properties of DM — assuming that the phenomenon is explained by a particle — requires it to have mass (so that it can interact gravitationally), it cannot interact with the known particles of the SM too strongly (otherwise it could cool and would no long fit density profiles seen in observations), and it must be stable or decay with a lifetime greater than the current age of the universe. There are also additional constraints coming from the

aforementioned astrophysical observations. For example, ensuring enough DM is left after the cooling of the early universe in order to explain the observed DM densities, known as the relic density or relic abundance, is a very basic requirement for any realistic model of DM. Initially, it seemed that neutrinos might be able to solve the DM problem, but it is now known that the neutrinos have too large of a free-streaming length in the early universe and thus they prevent the formation of large scale structure [35, 36].

One common model of DM is to have a new particle (often a scalar or a fermion though possible a vector boson) which is massive, interacts through the weak interaction or with a strength of interaction at the weak scale, and is stabilized through the addition of a new discrete symmetry (such as a Z_2 or R parity) so that the lightest of these new particles cannot decay to the SM particles [37]. These so called Weakly Interacting Massive Particles (WIMPs), can be accommodated in a wide variety of models, and are the typical example of cold DM (CDM). These WIMPs are appealing because of the so-called "WIMP miracle" where a choice in mass and choice of coupling constant for a particle near the weak scale reproduces the correct relic abundance, however it is also possible to achieve a "WIMPless miracle" [38]. Additionally, WIMPs are expected to be detectable via nuclei scattering experiments, making them an appealing candidate for DM [39]. However, there have been no definitive detection of WIMP DM particles, and experiments such as LUX have significantly reduced the parameter space for WIMP models [40].

Despite the appeal of WIMPs, there are several challenges that make alternative models of DM compelling. In particular, dwarf galaxies are observed to have a different density of DM compared to predictions from CDM models [41–44], and also fewer dwarf galaxies than what is expected from CDM models have been observed — although more dwarf galaxies have been discovered recently around the Milky Way [45]. If DM interacts relatively strongly with itself, it is possible to explain these dwarf galaxy observations and also may be a source of explanation for the Fermi-LAT gamma ray excess [46]. These observations make it clear that, beyond solving the DM problem, it is also important for particle physicists to investigate various paradigms of DM beyond WIMPs.

2.3 Neutrino Mass and Oscillation

2.3.1 Introduction

It has been firmly established that neutrinos undergo flavor oscillation, necessarily implying that neutrinos have nonzero masses [11, 12, 14–19, 47, 48]. Assuming that the neutrinos are a Dirac fermion, then this mass term is possible if a right-handed neutrino is added to the minimal SM particle content. Currently, there is a lack of evidence for the existence of a right-handed neutrino or a left-handed anti-neutrino. Particularly, from the invisible Z boson decay width measured at LEP [20] the number of neutrinos that couple to the Z boson are given by

$$N_\nu = 2.9841 \pm 0.0083. \tag{2.1}$$

If any right-handed neutrinos exist they essentially have to be sterile, that is non-interacting with the rest of the SM. Instead of being a Dirac fermion, the neutrino could also be what is called a Majorana fermion. Introduced in 1937 [49], Majorana particles are their own anti-particles, and could allow the neutrino to acquire a mass using different mechanisms thatn if it were a Dirac particle. As opposed to the typical Dirac fermion terms of $\bar{\psi_L}\psi_R$ the Marjorana mass terms are of the form $\bar{\psi_L}\psi_L^c$; and so a Majorana mass term could produce neutrino mass without requiring right-handed neutrinos. In 1979, Weinberg proved that there is a unique, dimension-five operator that generates a Majorana neutrino mass [50]:

$$\mathcal{L}_5 = \frac{-f_{ij}}{2\Lambda}(\nu_i\phi^0 - l_i\phi^+)(\nu_j\phi^0 - l_j\phi^+) + \text{h.c.} \tag{2.2}$$

After spontaneous symmetry break the Higgs receives a a nonzero expectation value $\langle\phi\rangle = v$, the neutrinos gain a Majorana mass given by $\frac{f_{ij}v^2}{\Lambda}$. Note that as the neutrinos carry a lepton number of 1, Majorana masses for the neutrino violate lepton number by 2. If the scale of the new physics, Λ, is large, then the neutrino mass is naturally small in a seesaw mechanism. As any terms in the Lagrangian with a dimension larger than five are non-renormalizable, the operator can be treated as an effective operator to some high-energy theory. For this

particular operator there are several ultraviolet (UV) completions that can be accomplished at tree-level. These UV completions at tree-level produce three different kinds of seesaw mechanisms, depending on the additional particles added to the SM:

1. Majorana fermion singlets N_i [51–53]
2. heavy scalar triplet $(\xi^{++}, \xi^{+}, \xi^{0})$ [54, 55]
3. heavy Majorana fermion triplets $(\Sigma^{+}, \Sigma^{0}, \Sigma^{-})$ [56]

In addition to tree-level realizations, there are also one-loop and two-loop realizations of the operator. A systematic study in Ref. [57] classifies one-loop neutrino mass mechanisms into three distinct mechanisms of generating neutrino mass via the five-dimensional operator in Eq. 2.2. Of particular note among the one-loop models are the Zee model and the scotogenic model. In the Zee model the Higgs sector is expanded to include two Higgs doublets, as well as a charged scalar with $L = -2$ lepton number assignment [58]. In the scotogenic model, there is also an additional doublet, but instead of a lepton number carrying scalar, there is a neutral fermion that may or may not carry lepton number [32]. Additionally, it is possible in the scotogenic model of Ref. [32] that the masses of the new particles allow what is known as the inverse seesaw [59, 60], where the neutrino mass is proportional the masses of new particles. While there are only a handful of tree, and one-loop level, operators to generate neutrino mass there are many different specific models that accommodate this new particle content.

Unlike with the leptons — where the hierarchy and absolute mass scales are well established — both the scale, and the ordering of the neutrino mass states are constrained, but unknown. Astrophysical measurements from WMAP and Planck place strong constraints on the sum of the neutrino masses — $\sum m_\nu < 0.17$ eV (*Planck*, TT,TE,EE+lowP+BAO [21]). However, the hierarchy of the neutrino masses is still unknown. If the neutrinos oscillate, this indicates that the flavor eigenstates that determine scattering and production of

neutrinos can be written as a superposition of the mass eigenstates:

$$\mid \nu_l\rangle = \sum_j U^*_{lj} \mid \nu_j\rangle, \tag{2.3}$$

with $l = e, \mu, \tau$ and U is the neutrino mixing matrix proposed by Pontecorvo, Maki, Nakagawa, and Sakata [61, 62] is referred to as the PMNS matrix. The PMNS matrix can be written in the Particle Data Group (PDG) convention as [10]:

$$\begin{pmatrix} c_{12}c_{13} & s_{12}c_{13} & s_{13}e^{-i\delta} \\ -s_{12}c_{23} - c_{12}s_{23}s_{13}e^{i\delta} & c_{12}c_{23} - s_{12}s_{23}s_{13}e^{i\delta} & s_{23}c_{13} \\ s_{12}s_{23} - c_{12}c_{23}s_{13}e^{i\delta} & -c_{12}s_{23} - s_{12}c_{23}s_{13}e^{i\delta} & c_{23}c_{13} \end{pmatrix} \times diag(1, e^{i\frac{\alpha_{21}}{2}}, e^{i\frac{\alpha_{31}}{2}}), \tag{2.4}$$

where c_{ij} and s_{ij} represent cosine and sine of the mixing angle between the i and jth mass eigenstate respectively. For more information on neutrino oscillation see Ref. [10]. It is important to note that it is possible to have three complex phases in the neutrino sector where δ is the Dirac CP violating phase, and α_{21} and α_{31} are the Majorana CP violating phases. These phases would exist in the case where neutrinos are Majorana particles. If the neutrinos are Majorana in nature, then β decay can occur without the emission of neutrinos, and this amplitude is proportional to the effective Majorana mass parameter m_{ee}, which is given by [10]

$$|m_{ee}| = |m_1 U^2_{e1} + m_2 U^2_{e2} + m_3 U^2_{e3}|. \tag{2.5}$$

While mass is necessary to produce neutrino oscillations the structure of this oscillations is not necessarily determined by any seesaw mechanisms. In fact, the observed oscillation in the lepton sector indicates that the charged leptons essentially do not oscillate, while the neutrinos have significant oscillations. Understanding the structure of this neutrino oscillation has opened up many interesting avenues of theoretical and experimental investigation.

2.3.2 Flavor Symmetry

Before the observation of neutrino oscillation angle θ_{13} [47, 48], the mixing matrix for neutrinos was consistent with the so-called tribimaximal mixing matrix proposed by Harrison, Perkins, and Scott [63]:

$$\begin{pmatrix} \sqrt{2/3} & \sqrt{1/3} & 0 \\ \sqrt{1/6} & \sqrt{1/3} & \sqrt{1/2} \\ \sqrt{1/6} & \sqrt{1/3} & \sqrt{1/2} \end{pmatrix} \tag{2.6}$$

Compared to the CKM matrix, which is well described by the Wolfenstein parameterization where the off-diagonals are small values, the mixing angles in the neutrino sector have two large angles($_{12}$,θ_{23}), and one comparatively smaller angle ($_{13}$) [10]. Additionally, the mass splitting between the charged leptons is very large compared to the experimental values for the neutrino masses. This near degeneracy of neutrino masses, along with the pattern of two large mixing angles and one smaller mixing angle, indicate either large amounts of fine-tuning or the existence of some underlying flavor symmetry. However, any such flavor symmetry must be broken by the charged leptons in order to explain the large mass splitting. A promising area of study has been the use of non-Abelian discrete groups to explain the lepton sector mixing. These non-Abelian discrete groups have higher dimensional representations, as well as several distinct one dimensional representations (see Appendix C for a brief review of group theory and relevant non-Abelian discrete group properties). By organizing the left-handed leptons into non-trivial representations of the discrete group, and the right-handed charged leptons into the various one-dimensional representations, it is possible to form invariants under the non-Abelian flavor symmetry that allow for the mismatch between charged and neutral leptons as well as fixing the form of the neutrino mixing matrix to be either exactly tribimaximal or approximately tribimaximal [3, 6, 64–68]. This has been studied in many contexts, and with many different discrete groups, but perhaps the simplest example utilizes the tetrahedral group also known as A_4. The A_4 group has

4 irreducible representations: $\mathbf{1}$, $\mathbf{1}'$, $\mathbf{1}''$, and $\mathbf{3}$. These representations obey the following multiplication rules

$$\mathbf{3} \times \mathbf{3} = \mathbf{1} + \mathbf{1} + \mathbf{1} + \mathbf{3} + \mathbf{3}, \tag{2.7}$$

$$\mathbf{1} \times \mathbf{1}' = \mathbf{1}'', \tag{2.8}$$

$$\mathbf{1}' \times \mathbf{1}'' = \mathbf{1}, \tag{2.9}$$

which can be explicitly written out as seen in Appendix C. By assigning the charged, right-handed, leptons $\mathbf{1}$, $\mathbf{1}'$, and $\mathbf{1}''$ under A_4 and assigning $(\nu_i, l_i) \sim \mathbf{3}$ with the addition of two Higgs doublets so that $\Phi_i \sim \mathbf{3}$ it is then possible to generate a charged lepton mass matrix of the form [64]

$$\mathcal{M}_l = \begin{pmatrix} h_1 v_1 & h_2 v_2 & h_3 v_1 \\ h_1 v_2 & h_2 \omega v_2 & h_3 \omega^2 v_2 \\ h_1 v_3 & h_2 \omega^2 v_3 & h_3 \omega v_3, \end{pmatrix} \tag{2.10}$$

where h_is are the Yukawa coupling constants, and v_is are the nonzero vacuum expectation value (VEV) of the Higgs doublets Φ_is after spontaneous symmetry breaking. If $v_1 = v_2 = v_3 = v$, then this mass matrix is diagonalized by [64]

$$U_L^\dagger \mathcal{M}_l U_R = \begin{pmatrix} \sqrt{3} h_1 v & 0 & 0 \\ 0 & \sqrt{3} h_2 v & 0 \\ 0 & 0 & \sqrt{3} h_3 v \end{pmatrix}, \tag{2.11}$$

where

$$U_L = \frac{1}{\sqrt{3}} \begin{pmatrix} 1 & 1 & 1 \\ 1 & \omega & \omega^2 \\ 1 & \omega^2 & \omega \end{pmatrix}, \; U_R = \begin{pmatrix} 1 & 0 & 0 \\ 0 & 1 & 0 \\ 0 & 0 & 1 \end{pmatrix}. \tag{2.12}$$

The neutrino mass is then generated by another mechanism — namely one of the three tree-level seesaws or any number of radiative mechanisms — where the additional particles are assigned various representations under A_4. If the neutrino mass matrix $\mathcal{M}_\nu$ isn't exactly

diagonalized by the tribimaximal matrix, and if these deviations away from tribimaximal are relatively small, then the mass matrix in the tribimaximal basis can be diagonalized using [69]

$$U_\epsilon \approx \begin{pmatrix} 1 & \epsilon_{12} & \epsilon_{13} \\ -\epsilon_{12}^* & 1 & \epsilon_{23} \\ -\epsilon_{13}^* & -\epsilon_{23}^* & 1, \end{pmatrix} \tag{2.13}$$

where the full neutrino mass matrix is given by

$$U' = U_{TB} U_\epsilon^{\mathrm{T}}, \tag{2.14}$$

where U' is in the tribimaximal basis and must have its phases rotated to be in the PDG convention. Given the relationship in Eq. 2.14, the physical neutrino mixing angles can be extracted [69] (in the PDG convention) via

$$\tan^2\theta_{12} = |U'_{e1}/U'_{e2}|^2,\ \tan^2\theta_{23} = |U'_{\mu 3}/U'_{\tau 3}|^2,\ |\sin\theta_{13}| = |U'_{e3}|, \tag{2.15}$$

where the Dirac CP violating phase δ can be extracted using the Jarlskog invariant [10], or with careful rotation of the Majorana phases of U'. This generic framework is only applicable when the off-diagonal elements of $\mathcal{M}_\nu$ in the tribimaximal basis are small, however depending on the flavor structure of the mechanism generating neutrino mass these elements may be sizeable compared to one, or alternatively the matrix can be block-diagonal and a simple 2x2 rotation matrix can be used. It important to note that, while the tribimaximal matrix is not exactly correct, the mixing angle between the m_1 and m_3 mass states means the electron flavored neutrino is predominantly a combination of the m_1 and m_2 masses. The hierarchy of these masses is still not known, but it is still possible the neutrinos obey the inverted hierarchy where $m_2 > m_1 > m_3$ which make the electron neutrino the heaviest in direct contradistinction to the charged lepton sector where the electron is the lightest of the leptons. Determining the hierarchy of the neutrino mass, determining whether or not θ_{23}

is maximal, determining the nature of neutrino mass (Majorana, Dirac, or pseudo-Dirac), measuring the value of the CP violation in the neutrino sector, and determining the absolute neutrino mass scale are all open experimental and theoretical problems of significant interest.

2.3.3 The Scotogenic Model of Neutrino Mass

The scotogenic model, is a one-loop model of neutrino mass first proposed in [32] that utilizes the interactions between the dark sector and neutrinos to create small neutrino masses. The model is a minimal extension of the Standard Model and only adds three neutral fermions ($N_{1,2,3}$), and a single SU(2) doublet (η), both of which are odd under an additional Z_2 symmetry (while the SM particles are even). The additional Z_2 symmetry prevents η from receiving a nonzero vacuum expectation value and allows N_i or η to act as a DM candidate particle. As a result, the tree-level neutrino masses are not possible, but a loop-level Majorana mass can still occur. The relevant additional terms to the Lagrangian for neutrino mass are given by [32]:

$$\mathcal{L}_Y = f_{ij}(\phi^- \nu_i + \bar{\phi}^0 l_i) l_j^c + h_{ij}(\nu_i \eta^0 - l_j \eta^+) N_j + \text{h.c.} \tag{2.16}$$

$$\mathcal{L}_V = \lambda_3 (\Phi^\dagger \Phi)(\eta^\dagger \eta) + \lambda_4 (\Phi^\dagger \eta)(\eta^\dagger \Phi) + \frac{1}{2}\lambda_5 ((\Phi^\dagger \eta)^2 + (\eta^\dagger \Phi)^2) \tag{2.17}$$

The above terms allow the radiative generation of neutrino mass, as seen in Fig. 2.1. After

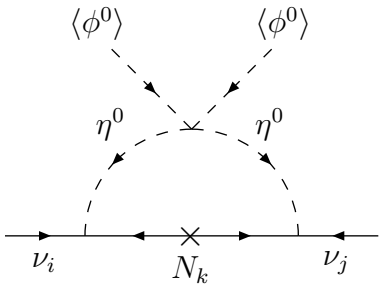

Figure 2.1: The minimal scotogenic mechanism of radiative neutrino mass.

ϕ^0 acquires a nonzero VEV (v) and using $\eta^0 = \eta_R + i\eta_I$, then the λ_5 term can be written as (dropping terms involving the electrically charged η components):

$$\frac{1}{2}\lambda_5 v^2(\eta_R^2 - \eta_I^2) \tag{2.18}$$

This term leads to an overall mass splitting between the real and imaginary components of the dark scalar doublet. Using the appropriate Feynman rules, then the scotogenic mass term is written as:

$$\pm\, h_{ij}h_{jk}\lambda_5 \int \frac{d^4k}{(2\pi)^4} \frac{(\not{k} + m_{N_j})}{(k^2 - m_\pm)(k^2 - m_{N_j})} \tag{2.19}$$

Where $m_\pm$ is the mass eigenstate of η_R and η_I respectively. Note the relative minus sign coming from the mass splitting between the real and imaginary components. As the tree-level mass is prevented, the loop generating the mass is guaranteed to be finite. The details of this integral can be found in Appendix A, but the resulting mass matrix is given by:

$$\mathcal{M}_{ij} = \sum_k \frac{h_{ik}h_{jk}}{16\pi^2}\left[\frac{m_R^2}{m_R^2 - M_k^2}\log\frac{m_R^2}{M_k^2} - \frac{m_I^2}{m_I^2 - M_k^2}\log\frac{m_I^2}{M_k^2}\right] \tag{2.20}$$

Taking different mass limits for m_R, m_I, and M_k this formula can produce both a seesaw and inverse seesaw like relation between the mass of M_k and that of the neutrino masses. If the η masses are greater than the neutral fermion masses then the following decays are

generically predicted [32]:

$$\eta^{\pm} \to l^{\pm} N_{1,2,3} \tag{2.21}$$

$$N_{2,3} \to l^{\pm} l^{\mp} N_{1,2} \tag{2.22}$$

This can lead to opposite-flavor opposite-sign dileptons plus missing energy, or even four lepton final states. And if the M_k are all greater than the η masses then the generic signature becomes:

$$N_{1,2,3} \to l^{\pm} \eta \mp \tag{2.23}$$

where the η can decay to the neutral scalar with a virtual W bosons. This can result in a variety of final states in a particle detector.

2.3.4 Extensions of Simplest Scotogenic Model

The minimal scotogenic model has been extended in many ways, and the concept of the scotogenic mechanism has been implemented in distinct one-loop mechanisms as well. With the additional of a discrete flavor symmetry, such as A_4, the model not only predicts the smallness of neutrino masses but also the nearly tribimaximal nature of neutrino oscillation [1]. The scotogenic model can also be extended for cases where the DM symmetry is a $U(1)$ gauge symmetry [4], or has its origin in lepton number [70]. The scotogenic mechanism has also been been studied with SU(5) gauge interactions [5] and SU(5) unification [71]. Alternative particle content in a scotogenic mechanism can also yield an inverse seesaw mechanism naturally [72].

Since the discovery of the 125 GeV Higgs Boson, and the lack of discovery of any other new physics at the 7 TeV and 8 TeV LHC runs, it has now become crucial to have models of new physics that can easily accommodate, or require, a Higgs boson that is very similar to the SM Higgs boson. Because the scotogenic model allows neutrino masses to gain a mass without directly coupling to the Higgs, it is an appealing framework to develop

rich phenomenology of new physics while utilizing a single SM-like Higgs Boson. In this vein, the model has also been extended to explain the lighter generations of lepton and quark masses. In order to extend the scotogenic mechanism to quark and lepton masses, it is necessary to have N added as a Dirac singlet fermion, with several additional charged scalars [73]:

1. A charged singlet χ^+
2. A color-triplet, SU(2) doublet $(\xi^{2/3}, \xi^{-1/3})$
3. A color-triplet, up-like, singlet $\zeta^{2/3}$
4. A color-triplet, down-like, singlet $\zeta^{-1/3}$.

All of the additional particles are part of the 'dark' sector, and can can carry 'dark' charge in a model with a $U(1)_D$ gauge symmetry. With suitible assignment under a flavor symmetry (for an example see Ref. [73]), then the lepton and quark masses are generated via the diagrams in Fig. 2.2 seen below. One intriguing aspect of the SM is that, because of the structure of weak interactions, there is a chiral anomaly in the quark and lepton sectors. However, this anomaly is neatly canceled as the quark sector anomaly cancels the lepton sector anomaly. This is suggestive that the quarks and leptons may unify at some high energy into a single irreducible representation of a unified gauge group. Particularly, it is well known that the SM quarks and leptons can be organized into the following SU(5) multiplets [10, 74]:

$$\mathbf{5}^* = d^c(3^*, 1, 1/3) + (\nu, e)(1, 2, -1/2) \tag{2.24}$$

$$\mathbf{10} = (u, d)(3, 2, 1/6) + u^c(3^*, 1, -2/3) + e^c(1, 1, 1). \tag{2.25}$$

By embedding the SM gauge group into a the Georgi-Glasho SU(5) representations [74], then at some very high energy there is a single unified gauge coupling. A theory that accomplishes this unification of gauge couplings is known as a Grand Unified Theory (GUT) (see Ref. [10] for a brief review on GUTs). In order to produce the proper spontaneous

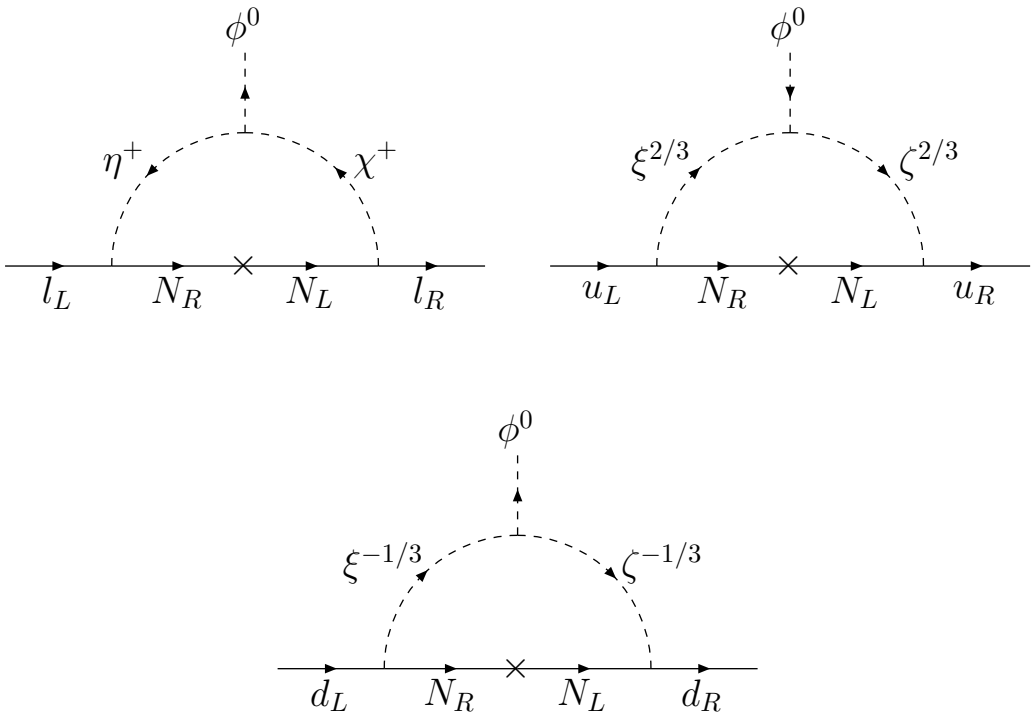

Figure 2.2: Unified scotogenic mechanism for quarks and leptons.

symmetry breaking at the weak scale, Higgs doublets are needed in either the **5** or irreducible representations of SU(5), with 3 additional states that are color triplet scalars [74]. These new particles are able to violate baryon and lepton number, and lead to very fast decay of stable matter (like protons) which pushes the mass of these new states to the 10^{11} GeV range [10]. Additionally, the simplest SU(5) GUT is ruled out from measurements of $\sin\theta_W$ and α_s, whereas supersymmetric SU(5) GUTs are potentially still viable [10]. It is also possible for an SU(5) theory to be embedded in a larger gauge group, such as SO(10), or the exception group E(6), and such more complicated non-SUSY GUTs are able to avoid problems with proton decay [75, 76]. With non-minimal GUTs that add additional scalars as **15** or **45** under SU(5) it is possible to avoid the constraints on non-SUSY GUTs [77]. These non-minimal theories generically predict light leptoquarks which may be found at the LHC [77, 78], however in order to reproduce the SM like Higgs the fine tuning

between light and massive particles organized into SU(5) multiplets is hard to avoid [78]. It is important to note that the unification of gauge couplings is not changed by adding or subtracting complete SU(5) multiplets. It is therefore possible to extend the scotogenic model of quark and lepton masses into an SU(5) theory [73], where $\eta, ^{-1/3} \sim \mathbf{5}$ and $(\xi^{2/3}, \xi^{-1/3}), (\zeta^{2/3})^*, \chi^+ \sim \mathbf{10}$, but gauge unification is achieved only if additional particles are added either in a non-minimal way [77,78], or in a supersymmetric context [71]. In this context, the fields are odd under an additional Z_2 that gives the DM candidates stability, in an analogy to R-parity in SUSY [73].

Part II

Flavor Symmetry, Neutrino Oscillation, and Collider Signatures

Chapter 3

Neutrino Oscillation Models

3.1 Heptagonic Flavor Symmetry for Quarks and Leptons

In the simplest implementations of neutrino oscillation — those arising in non-scotogenic models — the quark sector mixing isn't predicted by the flavor symmetry in the lepton sector. In fact, the mixing angles in the quark sector are predicted to be zero in strong conflict with experiment. It has been shown that the dihedral group of seven elements (D_7) can be utilized to produce both neutrino and quark oscillation data [2, 79]. This model requires several additional Z_2 symmetries, in addition to the extended particle content summarized below in Table 3.1. The up-like quark masses have Yukawa terms $uu^c\phi_7^0 + cc^c\phi_8^0$, while the down-like quark masses have the Yukawa terms $(ds^c + sd^c)\bar{\phi}_2^0$, $bb^c\bar{\phi}_2^0$, $b(d^c\bar{\phi}_4^0 + s^c\bar{\phi}_3^0), and (d\bar{\phi}_4^0 + s\bar{\phi}_3^0)b^c$. These Yukawa couplings produce a down-like quark mass matrix of the form

$$\mathcal{M}_d = \begin{pmatrix} 0 & a & \xi b \\ a & 0 & b \\ \xi c & c & d \end{pmatrix}, \tag{3.1}$$

where $\xi = \langle\bar{\phi}_4^0\rangle/\langle\bar{\phi}_3^0\rangle$ [2,79]. Following Ref. [79] the phases of $\mathcal{M}_d$ can be redefined such that a,b,c, and d are real but ξ is left as complex. The physical quark mixing matrix is found by

Particle	D_7	Z_2^d	Z_2^u	Particle	D_7	Z_2^d	Z_2^u
(u,d)	$\mathbf{2}_1$	+	+	Φ_2	$\mathbf{1}$	-	+
(c,s)	$\mathbf{2}_1$	+	+	$\Phi_{3,4}$	$\mathbf{2}_1$	-	+
(t,b)	$\mathbf{1}$	+	+	$\Phi_{5,6}$	$\mathbf{2}_2$	+	+
(d^c,s^c)	$\mathbf{2}_1$	-	+	$\Phi_{7,8}$	$\mathbf{2}_3$	+	-
b^c	$\mathbf{1}$	-	+	(ν_e,e)	$\mathbf{1}$	+	+
(u^c, c^c)	$\mathbf{2}_2$	+	-	(ν_μ,μ), (ν_τ,τ)	$\mathbf{2}_1$	+	+
(μ^c, τ^c)	$\mathbf{2}_3$	+	+	e^c	$\mathbf{1}$	+	+
t^c	$\mathbf{1}$	+	+	ζ_1	$\mathbf{1}$	+	+
Φ_1	$\mathbf{1}$	+	+	$\zeta_{2,3}$	$\mathbf{2}_1$	+	+

Table 3.1: D_7 Model Particle Content

$$V_L^\dagger \mathcal{M}_d \mathcal{M}_d^\dagger V_L = \begin{pmatrix} m_d^2 & 0 & 0 \\ 0 & m_s^2 & 0 \\ 0 & 0 & m_b^2 \end{pmatrix}. \tag{3.2}$$

Assuming that $a^2 \ll b^2$ and $|\xi|^2 \ll 1$ along with the form of $\mathcal{M}_d$ in Eq. 3.1 gives the following approximate expressions for the bottom quark mass and the V_{cb}, and V_{ub} components of the CKM matrix:

$$m_b \approx \sqrt{c^2 + d^2}, \tag{3.3}$$

$$V_{cb} \approx \frac{bd + \xi^* ac}{(1 + |\xi|^2)c^2 + d^2}, \tag{3.4}$$

$$V_{ub} \approx \frac{ac + \xi bd}{c^2 + d^2}. \tag{3.5}$$

Using these expressions, $\mathcal{M}_d$ can be transformed to be block-diagonal using

$$V_3 = \begin{pmatrix} 1 & 0 & V_{ub} \\ 0 & 1 & V_{cb} \\ -V_{ub}^* & -V_{cb}^* & 1 \end{pmatrix}, \tag{3.6}$$

yielding the following 2x2 matrix

$$\mathcal{M}_2\mathcal{M}_2^\dagger \begin{pmatrix} A & C \\ C^* & B \end{pmatrix}, \tag{3.7}$$

where

$$A = a^2 + |\xi|^2 b^2 - |V_{ub}|^2 m_b^2 \tag{3.8}$$

$$B = a^2 + b^2 - |V_{cb}|^2 m_b^2 \tag{3.9}$$

$$C = \xi b^2 - V_{ub}V_{cb}^* m_b^2. \tag{3.10}$$

Thus the remaining down-like masses and CKM parameter can be extracted:

$$m_s^2 = \frac{1}{2}(A+B) + \frac{1}{2}\sqrt{(A-B)^2 + 4|C|^2} \tag{3.11}$$

$$m_d = \frac{|2abc\xi - a^2 b|}{m_s m_b} \tag{3.12}$$

$$|V_{us}|^2 = \frac{1}{2}\left(1 - \sqrt{1 - \frac{4|C|^2}{(A-B)^2 + 4|C|^2}}\right), \tag{3.13}$$

where the phase of V_{us} is the same phase as the parameter C. Starting with $|V_{us}| = 0.22534$, then one immediately finds $\frac{|C|^2}{(A-B)^2} = 0.05971$. Given that, physically, $m_s^2 \gg m_d^2$ then $A \approx 0.05351B$ and thus $m_s^2 \approx 1.05359B$. By using this approximation it is possible to determine values of a, b, c, d, $Re(\xi)$, and $Im(\xi)$ that fit within the 2012 experimental limits of the CKM matrix elements, and the quark masses [2]. For the numerical analysis in Ref. [2], the approximation was used as a starting place for a full numerical scan of the allowed parameter space, but the final numerical solutions that diagonalize the mass matrix $\mathcal{M}_d$ did not depend on the approximate solutions. The parameters a,b, c, d $Re(\xi)$, and $Im(\xi)$ are varied until the 3 down-like quark masses and 3 mixing angles fit within one standard deviation of the 2012 PDG best-fit values for the CKM and the 2008 values of the down-like quark masses evaluated at M_W found in Ref. [80]. These values from the 2012

PDG are

$$|V_{us}| = 0.22535 \pm 0.00065, \tag{3.14}$$

$$|V_{cb}| = 0.0412 \begin{array}{c} +0.0011 \\ -0.0005 \end{array}, \tag{3.15}$$

$$|V_{ub}| = 0.00351 \begin{array}{c} +0.00015 \\ -0.00014 \end{array}, \tag{3.16}$$

and the down-like quark masses evaluated at M_W are

$$m_d(M_W) = 2.93 \begin{array}{c} +1.25 \\ -1.21 \end{array} \text{ MeV}, \tag{3.17}$$

$$m_s(M_W) = 56 \pm 16 \text{ MeV}, \tag{3.18}$$

$$m_b(M_W) = 2.92 \pm 0.09 \text{ GeV}. \tag{3.19}$$

The PDG also lists a condition that the ratio of the strange quark to down quark masses is in the range $17 < \frac{m_s}{m_d} < 22$ [81], and also limits the CP violating phase in the quark sector using the Jarlskog Invariant (J) [81, 82]

$$J = Im(V_{us}V_{cb}V_{ub}^*V_{cs}^*) = 2.96 \begin{array}{c} +0.20 \\ -0.16 \end{array} \times 10^{-5}. \tag{3.20}$$

The result of this numerical analysis is a prediction of the CP violating parameter J along

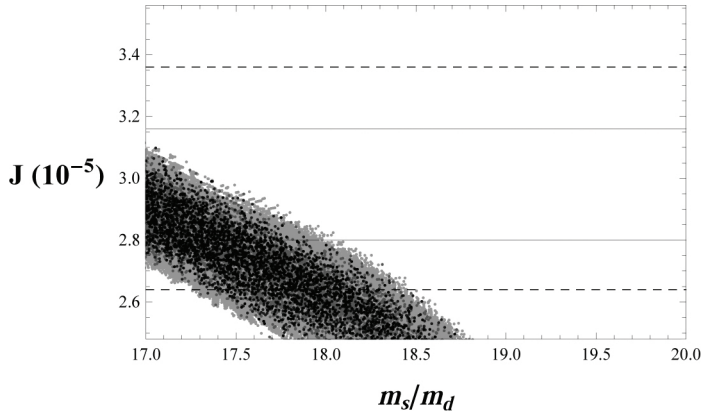

Figure 3.1: The CP violating parameter J versus m_s/m_d. The solid (dashed) lines indicate the one (two) standard deviation bounds of J.

Solution	m_d	m_s	m_b	$\mid V_{us} \mid$	$\mid V_{ub} \mid$	$\mid V_{cb} \mid$	J	m_s/m_d
I	3.89	66.2	292	0.22535	0.00355	0.0420	2.95×10^{-5}	17.00
II	3.91	67.4	293	0.22532	0.00358	0.0420	2.89×10^{-5}	17.25
III	3.96	69.2	296	0.22519	0.00363	0.0409	2.76×10^{-5}	17.50
IV	3.94	69.9	291	0.22501	0.00359	0.0415	2.70×10^{-5}	17.75

Table 3.2: D_7 resulting quark masses, mixing elements, and CP violating parameter J for four representative D_7 parameter solutions. Quark masses are in MeV.

Solution	a (GeV)	b (GeV)	c (GeV)	d (GeV)	$Re(\xi)$	$Im(\xi)$
I	0.0125	0.138	1.32	-2.60	0.053	-0.084
II	0.0124	0.139	1.34	-2.60	0.058	-0.084
III	0.0123	0.138	1.40	-2.60	0.064	-0.087
IV	0.0122	0.138	1.39	-2.55	0.068	-0.084

Table 3.3: D_7 representative parameter fits for quark masses and mixing.

with the ratio of m_s/m_d, as shown in Fig. 3.1. Several representative solutions of the physical quark masses, CKM matrix elements, along with the Jarlskog Invariant and the ratio of m_s/m_d are shown in Table 3.2, while the parameters a, b, c, d, $Re(\xi)$, and $Im(\xi)$ that produce these values are listed in Table 3.3. In addition to the predictions for the quark sector, the D_7 model detailed in Ref. [2] also has predictions for the neutrino sector which will not be detailed here.

As is immediately obvious from the listed particle content: this model of quark and lepton masses requires a very large number of Higgses that receive nonzero VEVs. The 125 GeV Higgs boson that was recently observed at the LHC [7, 8] appears to be mostly like the SM Higgs with no hints of exotic scalars at the electroweak scale. A model with so many Higgses is not guaranteed to produce an SM-like Higgs and is highly unlikely to be realized in nature. The structure provided by the flavor symmetry isn't enough to justify the large amount of fine-tuning that would be necessary to even determine if the model is consistent with a 125 GeV Higgs without taking into account the non-observation of novel physics at 7 TeV and 8 TeV LHC runs. In order for future models of flavor symmetry to be successful, it is necessary to naturally accommodate only a single, SM-like, Higgs boson with other exotic scalars being found only at higher energies such as the 13 TeV LHC or beyond.

3.2 Scotogenic Model with A_4 Flavor Symmetry

As discussed previously in Section 2.3.3 — as well as in Appendix A — if the splitting between the real and imaginary scalars in the minimal scotogenic mechanism is small compared to their masses, and if this is small compared to the masses of the neutral fermions N_k, then a radiative seesaw is achieved. However, this only explains the smallness of neutrino mass and doesn't explain the observed structure of the neutrino oscillations or the mismatch between the charged and neutral leptons. One of the well known solutions is the use of the discrete, non-Abelian, flavor symmetries such as A_4 as discussed in Section 2.3.2. Since the scotogenic mechanism connects the mass matrix of N to the neutrino mass matrix, then the implementation of a discrete flavor symmetry has two, generic, consequences:

1. The Yukawa coupling constants h_{ij} — from the allowed interaction term $\eta\nu_i N_j$ — are restricted depending on the flavor symmetry assignment of η, ν, and N.

2. The form of the mass matrix for N's is also fixed by the flavor symmetry assignment

of N, and the texture of this matrix results in a particular form of the neutrino mass matrix (in the flavor symmetry basis).

The work in Ref. [1] represents a particular implementation of the scotogenic mechanism, in the radiative seesaw approximation (see Appendix A), using the non-Abelian discrete symmetry A_4 as a flavor symmetry. Under A_4, the η is a trivial singlet ($\eta \sim \mathbf{1}$), while the N's are organized into a triplet ($N_i \sim \mathbf{3}$). Under all of the symmetries in the model, the neutral fermions N can have a Majorana mass term, but because it is a triplet under A_4, the only allowed invariant for such a term is $N_i N_i$ and thus each N has the same Majorana mass. In addition to the basic scotogenic particle content several scalar singlets are added as an A_4 triplet $\sigma_i \sim \mathbf{3}$ and each receives a VEV $\langle \sigma_i \rangle$. Because these are triplets, the allowed Yukawa terms are of the form $\sigma_i N_i N_k$, where no indice is repeated. After the σ_i receive VEVs the following mass matrix is produced:

$$\begin{pmatrix} A & F & E \\ F & A & D \\ E & D & A \end{pmatrix} \tag{3.21}$$

The neutrino masses are related to the mass matrix of above via the scotogenic mechanism in the limit where the mass difference between $\Re(\eta)$ and $\Im(\eta)$ is small relative to the average of their masses (m_0), and $m_0 \ll m_{N_k}$ (as explained in Appendix A):

$$(\mathcal{M}_\nu)_{ij} = \frac{\lambda_5 v^2}{8\pi^2} \sum_k \frac{h_{ij} h_{jk}}{m_{N_k}} \left[\log \frac{m_{N_k}^2}{m_0^2} - 1 \right], \tag{3.22}$$

where $\sum_k h_{ik} h_{jk}^\dagger = |h|^2 \delta_{ij}$. However, the neutrino eigenstates $\nu_{1,2,3}$ are related to $N_{1,2,3}$ through an identity matrix. As a consequence, the full neutrino oscillation matrix is given by the matrix that diagonalizes the mass matrix in equation 3.21. If $E = F$, then 3.21 is exactly diagonalized by the tribimaximal mixing matrix. However, $F = -E$ can be maintained via an interchange symmetry [83], resulting in two non-zero off-diagonal elements in 3.21 after

transforming the matrix to the tribimaximal basis:

$$\begin{pmatrix} A+D & 0 & 0 \\ 0 & A & C \\ 0 & C & A-D \end{pmatrix}, \tag{3.23}$$

where $C = (E-F)/\sqrt{2} = \sqrt{2}E$. To obtain the masses m_{N_k} the matrix in 3.23 must be diagonalized, but since it only has two non-zero off-diagonals a simple rotation matrix can be used:

$$\mathcal{M}_N^{(1,2,3)} = \begin{pmatrix} 1 & 0 & 0 \\ 0 & \cos(\theta) & \sin(\theta)e^{i\phi} \\ 0 & -\sin(\theta)e^{-i\phi} & \cos(\theta) \end{pmatrix} \begin{pmatrix} A+D & 0 & 0 \\ 0 & A & C \\ 0 & C & A-D \end{pmatrix} \begin{pmatrix} 1 & 0 & 0 \\ 0 & \cos(\theta) & -\sin(\theta)e^{-i\phi} \\ 0 & \sin(\theta)e^{i\phi} & \cos(\theta) \end{pmatrix}$$

$$\mathcal{M}_{N_{\text{diag}}}^{1,2,3} = \begin{pmatrix} e^{i\alpha_1}M_3 & 0 & 0 \\ 0 & e^{i\alpha_2}M_2 & 0 \\ 0 & 0 & e^{i\alpha_3}M_3 \end{pmatrix} \tag{3.24}$$

Note the presence of three complex phases (α_i) which originate in the Majorana nature of the N mass. Choosing A to be positive and real — to match the PDG convention as mentioned in Ref. [1] — then C and D may both be complex and expanded as $C = C_R + iC_I$ and $D = D_R + iD_I$. From the matrix equations above this yields:

$$\tan\phi = \frac{C_R D_I - C_I D_R}{C_R(2A - D_R) - C_I D_I} \tag{3.25}$$

$$\tan 2\theta = \frac{2(4A^2C_R^2 - 4AC_R(C_R D_R + C_I D_I) + (C_R^2 + C_I^2)(D_R^2 + D_I^2))^{1/2}}{2AD_R - (D_R^2 + D_I^2)} \tag{3.26}$$

$$e^{i\alpha_2}M_2 = A\cos^2\theta + 2C\sin\theta\cos\theta e^{i\phi} + (A-D)\sin^2\theta e^{i2\phi} \tag{3.27}$$

$$e^{i\alpha_3}M_3 = (A-D)\cos^2\theta - 2C\sin\theta\cos\theta e^{-i\phi} + A\sin^2\theta e^{-i2\phi} \tag{3.28}$$

To find the U_{PMNS} matrix, we multiply the tribimaximal matrix by the 3x3 rotation matrix above which yields:

$$U'_{e1} = \sqrt{\frac{2}{3}}, \quad U'_{e2} = \frac{\cos\theta}{\sqrt{3}}, \quad U'_{e3} = -\frac{\sin\theta}{\sqrt{3}}e^{-i\phi}$$
$$U'_{\mu 3} = -\frac{\cos\theta}{\sqrt{2}} - \frac{\sin\theta}{\sqrt{3}}e^{-i\phi}, \quad U'_{\tau 3} = \frac{\cos\theta}{\sqrt{2}} - \frac{\sin\theta}{\sqrt{3}}e^{-i\phi}$$

Taking these mass matrix elements, it is possible to extract the relationship between θ and ϕ and neutrino mixing angles and the Dirac phase through the procedure explained in Refs. [1, 69] and in Section 2.3.2. The three angles are given by:

$$\tan^2\theta_{12} = |U'_{e2}/U'_{e1}|^2 = \frac{\cos^2\theta}{2} \tag{3.29}$$
$$\tan^2\theta_{23} = |U'_{\mu 3}/U'_{\tau 3}|^2 = \frac{1/2 + \cos\theta\sin\theta\cos\phi}{1/2 - \cos\theta\sin\theta\cos\phi} \tag{3.30}$$
$$\sin\theta_{13}e^{-i\delta_{CP}} = U'_{e3}e^{-i\alpha_3/2} = -\frac{\sin\theta}{\sqrt{3}}e^{-i(\phi+\alpha_3/2)} \tag{3.31}$$

For the purposes of the analysis the scale-factor $\frac{\lambda_5 v^2 h^2}{8\pi^2}$ is absorbed into the A, C, and D parameters and the mass m_0 so the neutrino masses from Eq. 3.22 is reduced to

$$m'_k = \frac{1}{m_{N_k}}\left[\log\frac{m^2_{N_k}}{m^2_0} - 1\right]. \tag{3.32}$$

where M_{N_k} are given by

$$M_{N_1} = |A + D| \tag{3.33}$$
$$M_{N_2} = \left(A\cos^2\theta + 2C\cos\theta\sin\theta e^{i\phi} + (A - D)\sin^2\theta e^{i2\phi}\right)e^{-i\alpha'_2} \tag{3.34}$$
$$M_{N_3} = \left((A - D)\cos^2\theta - 2C\theta\sin\theta e^{-i\phi} + A\sin^2\theta e^{-i2\phi}\right)e^{-i\alpha'_3} \tag{3.35}$$

The mass m_0 is the DM scalar mass and is unknown, so it is fixed by requiring $m_{N_1}/m_0 = 10$. The differences in the neutrino masses were taken to fall in the following ranges:

$$\Delta m^2_{21} = 7.59 \times 10^{-5}\text{eV}^2, \quad \Delta m^2_{32} = 2.45 \times 10^{-3}\text{eV}^2, \tag{3.36}$$

and the mixing angle θ_{13} is varied in the range

$$\sin^2 2\theta_{13} = 0.05 - 0.15, \tag{3.37}$$

and, following Ref. [69], $\sin^2 2\theta_{23}$ is fixed as either 0.92 or 0.96. The texture of the mass

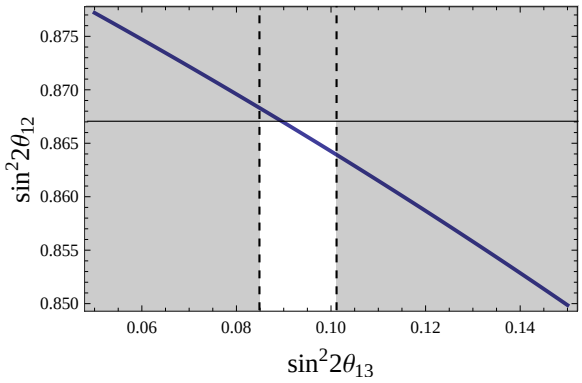

Figure 3.2: $\sin^2(2\theta_{12})$ versus $\sin^2(2\theta_{23})$, shaded area is ruled out at one standard deviation in 2014 PDG neutrino oscillation data.

matrix $\mathcal{M}_N$ is the same as that found in Ref. [69], and so the predictions of the mixing angles in Ref. [1] are the same as in Ref. [69] as illustrated in Fig. 3.2. As a consequence C must have an imaginary component (otherwise θ_{23} is too small), and the mixing angle ϕ is required to satisfy $|\tan\phi| > 1.2$ if $\sin^2(2\theta_{23}) > 0.92$. It is important to note that the values used for this analysis are not the current best-fit results found in the PDG review of neutrino oscillations, but at the time of publication the values used in Ref. [1] were the PDG best-fit values. To expedite the numerical analysis of the model, the mass hierarchy and

θ_{23} are fixed. To fit the neutrino mass differences and the mixing angles it is necessary

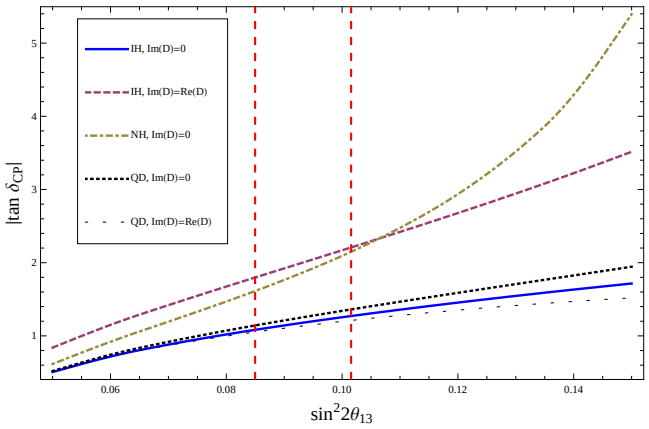

Figure 3.3: Prediction of the Dirac CP phase $|\tan\delta_{CP}|$ versus $\sin^2(2\theta_{13})$ for inverted (IH), normal (NH), and quasi-degenerate (QD) neutrino mass hierarchies. Red lines represent one standard deviation range in 2014 PDG neutrino oscillation data.

to solve Eq. 3.32 for the parameters A, B, C_R, C_I, D_R, and D_I, however the logarthim makes this equation very non-trivial. However, this term is expected to be of order unity and by dropping it the simpler equation can be exactly inverted, and the mass parameters that produce the correct mixing angles and physical neutrino masses can be found. The neighborhood around these approximate values are scanned to numerically determine the full solutions for the physical neutrino masses without using the approximation. After these solutions are determined the CP violating phases (1 Dirac, 2 Majorana) and the neutrinoless double-beta decay parameter m_{ee} are predicted. To further simplify the parameter space, the analysis is split into two solutions where the parameter D is purely real and another where $D_R = D_I \neq 0$. For the choice of a pure real D then inverted, normal, and quasi-degenerate mass hierarchies allowed, while for $D_R = D_I$ only inverted and quasi-degenerate

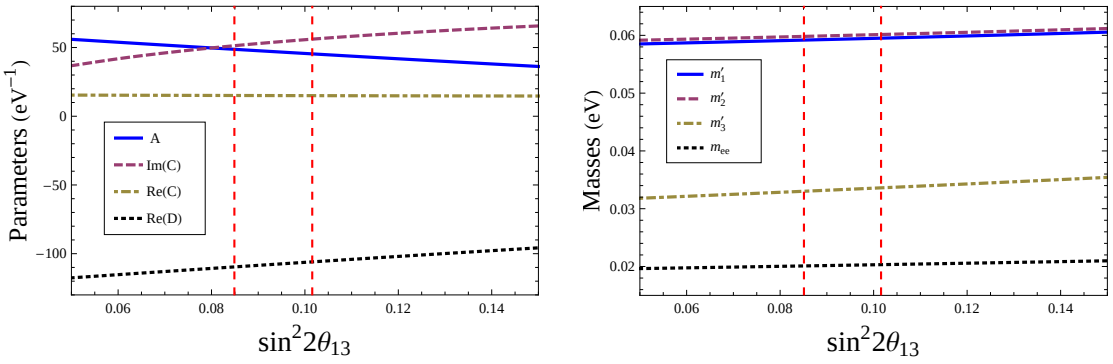

Figure 3.4: $\mathcal{M}_N$ parameters and the physical neutrino masses versus $\sin^2(2\theta_{13})$ in the case of inverted mass hierarchy, $D_I = 0$, and $\sin^2(2\theta_{23}) = 0.96$. Red lines represent one standard deviation range in 2014 PDG neutrino oscillation data.

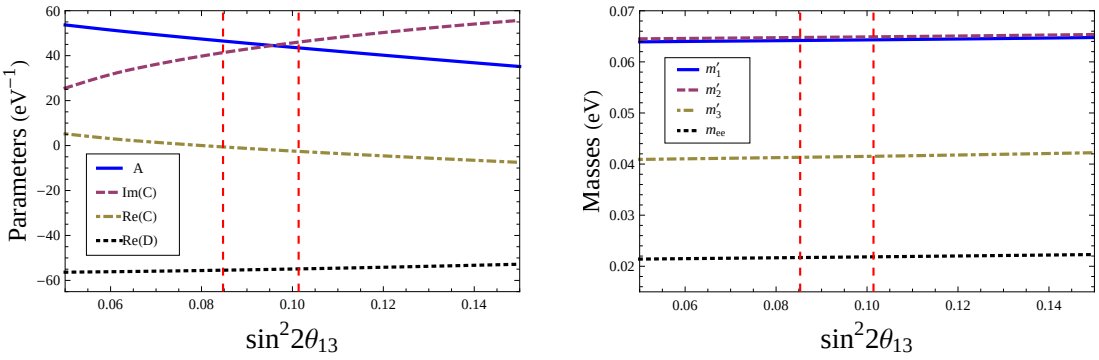

Figure 3.5: $\mathcal{M}_N$ parameters and the physical neutrino masses versus $\sin^2(2\theta_{13})$ in the case of inverted mass hierarchy, $D_I = D_R$, and $\sin^2(2\theta_{23}) = 0.92$. Red lines represent one standard deviation range in 2014 PDG neutrino oscillation data.

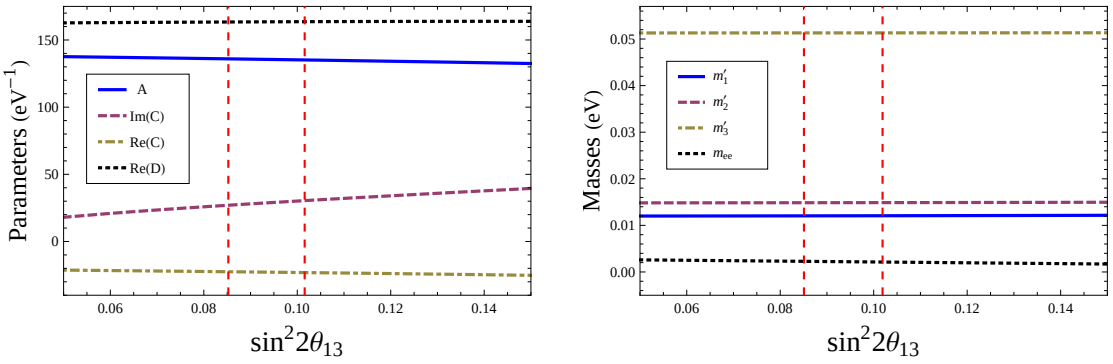

Figure 3.6: $\mathcal{M}_N$ parameters and the physical neutrino masses versus $\sin^2(2\theta_{13})$ in the case of a normal mass hierarchy, and , $D_I = 0$, and $\sin^2(2\theta_{23}) = 0.96$. Red lines represent one standard deviation range in 2014 PDG neutrino oscillation data.

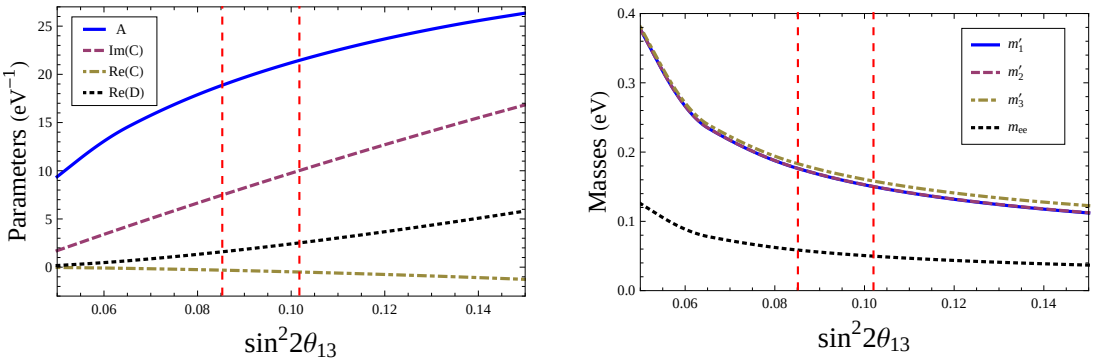

Figure 3.7: $\mathcal{M}_N$ parameters and the physical neutrino masses versus $\sin^2(2\theta_{13})$ in the case of quasi-degenerate mass hierarchy, $D_I = 0$, and $\sin^2(2\theta_{23}) = 0.92$. Red lines represent one standard deviation range in 2014 PDG neutrino oscillation data.

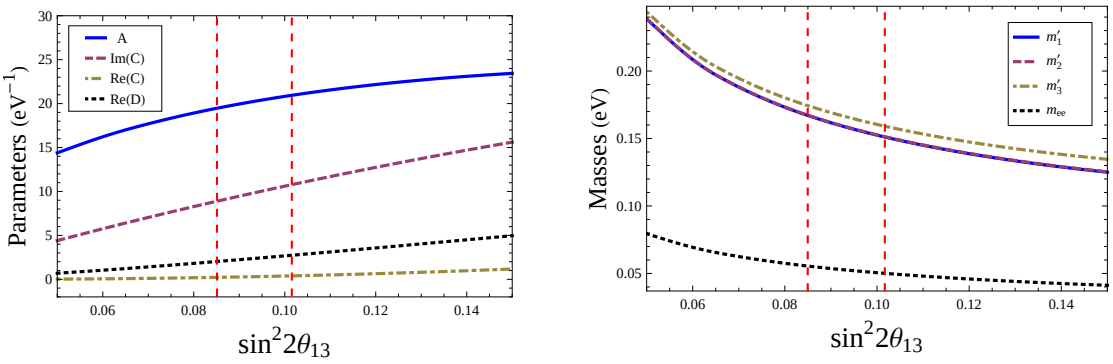

Figure 3.8: $\mathcal{M}_N$ parameters and the physical neutrino masses versus $\sin^2(2\theta_{13})$ in the case of quasi-degenerate mass hierarchy, $D_I = 0$, and $\sin^2(2\theta_{23}) = 0.96$. Red lines represent one standard deviation range in 2014 PDG neutrino oscillation data.

hierarchies are allowed. The full results of this analysis are seen in Figs. 3.4-3.8 for all three possible hierarchies, and for the two choices in $\sin^2(2\theta_{23}) = 0.92$ and 0.96. The correlation between the Dirac CP violating phase $|\tan\delta_{CP}|$ and $\sin^2(2\theta_{13})$ is illustrated in Fig. 3.3.

3.3 Scotogenic Model with $\Delta(27)$ Flavor Symmetry

In the previous section 3.2, the simplest scotogenic model was studied with the addition of an A_4 flavor symmetry, however there are many other discrete flavor symmetries that have been studied in the literature [84], and there are interesting extensions to the simplest scotogenic model as well as discussed in Section 2.3.4. Similar to proposals of other discrete flavor symmetries, $\Delta(27)$ can explain the difference in charged lepton masses while using an underlying symmetry to explain the mismatch of the charged and neutral lepton sectors and explain the pattern of neutrino oscillation. In addition, $\Delta(27)$ has been studied in the context of spontaneous CP violation where the theory at high energy is CP-invariant, but the vacuum obtains a CP violating phase. The use of $\Delta(27)$ to spontaneously break CP was first proposed in Ref. [85]. In this section, two particular implementations of $\Delta(27)$ are studied in two different scotogenic contexts — following the work presented in Ref. [4].

The non-Abelian discrete group $\Delta(27)$ has nine distinct one-dimensional representations $\mathbf{1_i}$ $(i = 1, \cdots, 9)$ and two three-dimensional representations $\mathbf{3}$ and $\mathbf{3}^*$. For group theoretic details on $\Delta(27)$ see the discussion in Appendix C. The three-dimensional representations have the following multiplication rules:

$$\mathbf{3} \times \mathbf{3}^* = \sum_{i=1}^{9} \mathbf{1_i}, \quad \mathbf{3} \times \mathbf{3} = \mathbf{3}^* + \mathbf{3}^* + \mathbf{3}^*. \tag{3.38}$$

As a result, $\mathbf{3} \times \mathbf{3} \times \mathbf{3}$ can form a trivial singlet in three distinct invariants:

$$111 + 222 + 333 \tag{3.39}$$

$$123 + 231 + 321 + (132 + 213 + 321) \tag{3.40}$$

$$123 + 231 + 321 - (132 + 213 + 321) \tag{3.41}$$

It is important to note that the complex conjugation of one of the three-dimensional representations yields the other, just as is the cse in SU(3). Following the discussion in Ref. [4], it is possible to assign the following representations of $\Delta(27)$ to the particle content of the simplest scotogenic model: $\Phi, \eta \sim \mathbf{1}_1$, $\nu \sim \mathbf{3}$, $N \sim \mathbf{3}^*$. Similar to the model in Ref. [1], there are additional neutral scalars that receive VEVs ζ; these additional scalars generate additional mass terms in the 3x3 Majorana mass matrix of the N_is and under $\Delta(27)$ are assigned $\mathbf{3}$. The Yukawa couplings are given by $f_{ijk} N_i N_k \zeta_k^*$. Using the above invariants in Eqs. 3.40 - 3.41, and given that each of the three $\zeta_{1,2,3}$ receive VEVs $\langle \zeta_i \rangle = v_{\zeta i}$, we can re-write the Yukawa terms using the above invariants such that:

$$f_1(11 v_{\zeta 1} + 22 v_{\zeta 2} + 33 v_{\zeta 3}) \tag{3.42}$$

$$f_2[(12 v_{\zeta 3} + 23 v_{\zeta 1} + 31 v_{\zeta 2}) + (13 v_{\zeta 2} + 21 v_{\zeta 3} + 32 v_{\zeta 1})] \tag{3.43}$$

For simplicity we can re-write the above terms with as $f_2 v_{\zeta 1,2,3} = a, b, c$ and $f_1/f_2 = f$:

$$f(11a + 22b + 33c) \tag{3.44}$$

$$12c + 23a + 31b + 13b + 21c + 32a, \tag{3.45}$$

just as was the case in A_4 the invariant terms must share the same Yukawa coupling constant. These terms can be quickly reorganized into a mass matrix for N, and diagonalizing this matrix will also diagonalize the neutrino mass matrix. Thus, the neutrino mass matrix with such a particle assignment under $\Delta(27)$ is of the form

$$\mathcal{M}_\nu = \begin{pmatrix} fa & c & b \\ c & fb & a \\ b & a & fc \end{pmatrix} \tag{3.46}$$

Instead of using a scotogenic model where the 'dark' symmetry is Z_2, it is of interest to consider cases where there is a 'dark' gauge symmetry $U(1)_D$. This 'dark' symmetry can be broken to a residual Z_2 or left as an exact symmetry as first discussed in a scotogenic context in Ref. [86]. Instead of usual scotogenic content, the 'dark' gauge symmetry requires the particle content to be modified with two additional scalar doublets (η_1^+, η_1^0) and (η_2^+, η_2^0) which have $+1$ and -1 'dark' charge respectively. The three neutral fermions N_i have $+1$ 'dark' charge and are Dirac fermions. For the generation of neutrino mass the relevant interaction terms are $h_1 \bar{N}_R \nu_L \eta_1^0$, $h_2 N_L \bar{\nu}_L^c \eta_2^0$, and $(\Phi^\dagger \eta_1)(\Phi^\dagger \eta_2)$; this last term allows mixing between the two additional scalars (η_1^0 and $\bar{\eta}_2^0$) which can be related to the mass eigenstates $\chi_{1,2}$ [86]:

$$\begin{pmatrix} \eta_1^0 \\ \bar{\eta}_2^0 \end{pmatrix} = \begin{pmatrix} \cos\theta & \sin\theta \\ -\sin\theta & \cos\theta \end{pmatrix} \begin{pmatrix} \chi_1 \\ \chi_2 \end{pmatrix} \tag{3.47}$$

Using Eq. 3.47 the Yukawa couplings can be re-written in terms of mass states

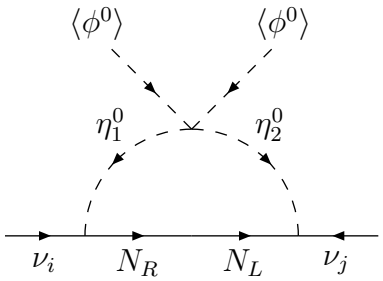

Figure 3.9: The scotogenic mechanism with $U(1)_D$ dark matter.

$$h_1 \bar{N}_R \nu_L (\cos\theta \chi_1 + \sin\theta \chi_2) \tag{3.48}$$

$$h_2 N_L \bar{\nu}_L^c (-\sin\theta \bar{\chi}_1 + \cos\theta \bar{\chi}_2) \tag{3.49}$$

Despite the neutral fermion N having a Dirac mass, the resulting neutrino mass is still Majorana, and the calculation of the neutrino mass procedes very similar to the minimal scotogenic model, however the mass splitting is coming from the relative minus sign between χ_1 and χ_2 in Eq. 3.49 as opposed to the relative minus sign between η_R and η_I that occurs in the minimal model. In addition, η_1 and η_2 can be permuted yielding two distinct diagrams that contribute to the physical mass. This permutation is taken into account with the sum of the permutation of Yukawa couplings seen in Eq. 3.50. This modified Scotogenic mechanism results in the neutrino mass matrix of the form

$$\begin{aligned}(\mathcal{M}_\nu)_{ij} = \cos\theta \sin\theta \sum_k \frac{(h_1)_{ki}(h_2)_{kj} + (h_2)_{ki}(h_1)_{kj}}{8\pi^2} \\ \times M_{N_k} \left[\frac{m_1^2}{m_1^2 - M_{N_k}^2} \log \frac{m_1^2}{M_{N_k}^2} - \frac{m_2^2}{m_2^2 - M_{N_k}^2} \log \frac{m_2^2}{M_{N_k}^2} \right],\end{aligned} \tag{3.50}$$

where $m_{1,2}$ are the masses of $\chi_{1,2}$. This modification of the scotogenic mechanism can also yield the neutrino mass matrix in Eq. 3.46 through the Yukawa coupling $f_{ijk}\bar{N}_{Li}N_{Rj}\zeta_k$ if the following representations in $\Delta(27)$ are assigned: $\Phi, \eta_{1,2} \sim \mathbf{1}_1$, $\nu \sim \mathbf{3}$, $N_R \sim \mathbf{3}$, and $N_L \sim \mathbf{3}^*$. A mass matrix of this form arising from a $\Delta(27)$ flavor symmetry has already

been studied in a non-scotogenic context in Refs. [67, 68]. In Ref. [67] the lepton singlet l^c is assigned the $\mathbf{3}^*$ representation while three additional Higgs doublets ($\phi_{1,2,3}$) are assigned $\mathbf{1}_{1,2,3}$ respectively, yielding a diagonal charged-lepton mass matrix. In [68] $l^c, \phi \sim \mathbf{3}$, and the charged-lepton sector is not diagonal [68], but is given by

$$\mathcal{M}_l = U_\omega \begin{pmatrix} m_e & 0 & 0 \\ 0 & m_\mu & 0 \\ 0 & 0 & m_\tau \end{pmatrix} U_\omega^\dagger, \tag{3.51}$$

where $\omega = e^{i2\pi/3}$ and U_ω is the Cabibbo-Wolfenstein matrix

$$U_\omega = \frac{1}{\sqrt{3}} \begin{pmatrix} 1 & 1 & 1 \\ 1 & \omega & \omega^2 \\ 1 & \omega^2 & \omega \end{pmatrix}. \tag{3.52}$$

Both the model in Ref. [67] and the model in Ref. [68] are consistent with $\theta_{13} \neq 0$, which was first determined experimentally in 2012, however of the two solutions presented in Ref. [67] only the solution where $f \approx -0.5$ is able to produce a realistic θ_{13}. To analyze the case with a diagonal lepton mass matrix in the scotogenic models (either Z_2 or $U(1)_D$ model), the parameters in the mass matrix are re-writtne as $f = -\frac{1}{2} + \epsilon$, $a = b(1+\eta)$, and $c = b(1-\kappa)$, then the mass matrix in the tribimaximal basis is

$$\mathcal{M}_\nu^{\mathrm{TB}} = U_{\mathrm{TB}}^{\mathrm{T}} \mathcal{M}_\nu U_{\mathrm{TB}} = \begin{pmatrix} -\frac{3}{2} + \epsilon + \frac{3}{4}\kappa & -\frac{2\eta+\kappa}{2\sqrt{2}} & \frac{\sqrt{3}}{4}\kappa \\ -\frac{2\eta+\kappa}{2\sqrt{2}} & \frac{3}{2} + \epsilon + \frac{1}{2}\eta + \frac{1}{2}\kappa & \frac{\sqrt{3}}{2\sqrt{2}}\kappa \\ \frac{\sqrt{3}}{4}\kappa & \frac{\sqrt{3}}{2\sqrt{2}}\kappa & -\frac{3}{2} + \epsilon - \eta + \frac{1}{4}\kappa \end{pmatrix} b, \tag{3.53}$$

where ϵ, η, and κ are all assumed to be small compared to one, that is the neutrino mass matrix is nearly diagonal in the tribimaximal basis. We define a new parameter ζ, such that $\zeta = \kappa + 2\eta$, and assume all parameters to be real. Given these assumptions, the mixing

matrix is nearly tribimaximal and can be diagonalized by

$$U' = \begin{pmatrix} 1 & \theta'_{12} & \theta'_{13} \\ -\theta'_{12} & 1 & \theta'_{23} \\ -\theta'_{13} & -\theta'_{23} & 1 \end{pmatrix}, \tag{3.54}$$

where $\theta'_{ij} = \frac{m_{ij}}{m_{ii}-m_{jj}}$, and m_{ij} are the matrix elements of 3.53, which yields the physical neutrino masses of the form

$$\Delta m^2_{21} \approx m^2_{22} - m^2_{11} \approx \frac{3}{4}(8\epsilon + \zeta)b^2 \tag{3.55}$$

$$\Delta m^2_{32} \approx m^2_{33} - m^2_{11} \approx \frac{3}{2}\zeta b^2, \tag{3.56}$$

and the physical mixing angles are determined by

$$U_{TB}U' = \begin{pmatrix} \sqrt{\frac{2}{3}} + \frac{\theta'_{12}}{3} & \frac{1}{\sqrt{3}} - \sqrt{\frac{2}{3}}\theta'_{12} & -\sqrt{\frac{2}{3}}\theta'_{13} - \frac{\theta'_{23}}{\sqrt{3}} \\ -\frac{1}{\sqrt{6}} + \frac{\theta'_{12}}{\sqrt{3}} - \frac{\theta'_{13}}{\sqrt{2}} & \frac{1}{\sqrt{3}} + \frac{\theta'_{12}}{\sqrt{6}} - \frac{\theta'_{23}}{\sqrt{2}} & -\frac{1}{\sqrt{2}} + \frac{\theta'_{13}}{\sqrt{6}} - \frac{\theta'_{23}}{\sqrt{3}} \\ -\frac{1}{\sqrt{6}} + \frac{\theta'_{12}}{\sqrt{3}} + \frac{\theta'_{13}}{\sqrt{2}} & \frac{1}{\sqrt{3}} + \frac{\theta'_{12}}{\sqrt{6}} + \frac{\theta'_{23}}{\sqrt{2}} & \frac{1}{\sqrt{2}} + \frac{\theta'_{13}}{\sqrt{6}} - \frac{\theta'_{23}}{\sqrt{3}} \end{pmatrix}, \tag{3.57}$$

which can be compared to the PDG parameterization by

$$\tan\theta_{12} = \frac{\sqrt{1/3} - \sqrt{2/3}\theta'_{12}}{\sqrt{2/3} + \sqrt{1/3}\theta'_{12}} \tag{3.58}$$

$$\sin\theta_{13} = \pm\left(\sqrt{\frac{2}{3}}\theta'_{13} + \sqrt{\frac{1}{3}}\theta'_{23}\right) \tag{3.59}$$

$$\tan\theta_{23} = \frac{1/\sqrt{2} + \theta'_{13}/\sqrt{6} - \theta'_{23}/\sqrt{3}}{-1/\sqrt{2} + \theta'_{13}/\sqrt{6} - \theta'_{23}/\sqrt{3}}. \tag{3.60}$$

Using the values from Eq. 3.53 and $\eta = \frac{\zeta - \kappa}{2}$, and dropping higher order terms, yields

$$\theta'_{12} = \frac{m_{12}}{m_{11} - m_{22}} \approx \frac{\zeta}{6\sqrt{2}} \tag{3.61}$$

$$\theta'_{13} = \frac{m_{13}}{m_{11} - m_{33}} \approx \frac{\sqrt{3}}{2}\frac{\kappa}{\zeta} \tag{3.62}$$

$$\theta'_{23} = \frac{m_{23}}{m_{22} - m_{33}} \approx \frac{\kappa}{2\sqrt{6}}, \tag{3.63}$$

and using Eqs. 3.59 - 3.60 the physical mixing angles are approximately given by:

$$\sin\theta_{13} \approx \pm\frac{\kappa}{\sqrt{2}\zeta} \tag{3.64}$$

$$\tan\theta_{12} \approx \frac{1}{\sqrt{2}}\left(\frac{1-\zeta/6}{1+\zeta/12}\right). \tag{3.65}$$

$$\tag{3.66}$$

It is important to note that the neutrino mass matrix in Eq. 3.53 is quasi-degenerate ($m_{11} \approx -m_{22} \approx m_{33}$), and as a result θ'_{23} is much smaller than θ'_{13}. In the limit that $\theta'_{23} = 0$, then

$$\tan\theta_{23} \approx 1 + \frac{\kappa}{\zeta}, \tag{3.67}$$

which yields

$$\sin^2 2\theta_{23} \approx 1 - 2\sin^2\theta_{13}, \tag{3.68}$$

which is consistent with the current experimental neutrino data. However, if θ'_{23} dominates then the relationship between θ_{23} and θ_{13} would be $1 - 8\sin^2\theta_{13}$, which is ruled out by data as first pointed out by Ref. [69]. By fixing θ_{12}, Δm^2_{31}, Δm^2_{21}, and $\sin\theta_{13}$ it is thus possible to find a prediction for θ_{23} and the neutrinoless double beta decay parameter m_{ee}. For example, a choice of $\tan^2\theta_{12} = 0.45$ results in $\zeta = 0.209$ and a normal mass hierarchy, and setting $\Delta m^2_{21} = 7.50 \times 10^{-5}\ eV^2$, $\sin\theta_{13} = 0.16$ results in $b = 0.086$ eV, $\sin^2 2\theta_{23} = 0.966$, and $m_{ee} = |fa| = 0.05$ eV. For these representative numerical values ζ is small but not much smaller than one. Additionally, with these values $\kappa = \pm 0.047$ and so κ/ζ is also on

the order of ζ and assuming this ratio is neglibile is no longer justifiable. Thus for the full numerical analysis the approximate solutions are used only as an initial solution for the mass matrix parameters b, ζ, κ, and ϵ. These input values are used as a guideline to focus the range of the parameter space scan, and the mass matrix is numerically diagonalized without assuming ζ, κ, or ϵ are much smaller than one. In addition, the case where κ is purely imaginary is considered in which $\sin^2 2\theta_{23} = 1$. This limit is guaranteed due to a symmetry that is based on a generalized CP transformation as discussed in Ref. [87]. For the numerical analysis the following values for the neutrino mixing parameters were used in Ref. [4]:

$$\Delta m^2_{21} = 7.50 \pm 0.20 \times 10^{-5}\text{eV}^2, \tag{3.69}$$

$$\Delta m^2_{32} = 2.32 + 0.12 - 0.08 \times 10^{-3}\text{eV}^2, \tag{3.70}$$

$$\sin^2 2\theta_{12} = 0.857 \pm 0.025, \tag{3.71}$$

$$\sin^2 2\theta_{23} > 0.95, \tag{3.72}$$

$$\sin^2 2\theta_{13} = 0.095 \pm 0.010. \tag{3.73}$$

To determine the CP violation in this mass matrix, the Jarlskog Invariant [82] is used, which can be related to the Dirac CP violating phase δ via

$$J_{CP} = Im(U_{\mu 3} U^*_{e3} U_{e2} U^*_{\mu 2}), \tag{3.74}$$

where $U_{i\alpha}$ are the elements of the neutrino mixing matrix in the PDG convention. As κ is varied between purely real and purely imaginary, $\sin^2 2\theta_{23}$ slowly increases from 0.966 (purely real κ) to 1 (purely imaginary κ). Using the current PDG values for $\sin^2 \theta_{23}$ puts this value for a purely real κ a little less than two sigma away from the best-fit value [10]. For the analysis of the neutrinoless double beta decay parameter (m_{ee}) $\sin^2 2\theta_{13}$ was varied between the values in Eq. 3.73 and κ was allowed to vary arbitrarily between purely real and purely imaginary. For the analysis of J_{CP} a purely imaginary κ was used, and $\sin^2 2\theta_{12}$ was

varied between the values in Eq. 3.72, and $\sin^2\theta_{23}$ was determined to be one, as required. The results of the analysis indicate that m_{ee} is mostly sensitive to variations in θ_{12} whereas $J_{\rm CP}$ is mostly sensitive to variations in θ_{13}. In Figs. 3.10 3.11 these results are plotted, and the sensitivity to different angles is demonstrated. In Fig. 3.10, the upper band represents the purely real κ solutions, and the lower band represents the purely imaginary κ solutions. Points in the region in between these two bands are allowed for arbitrary choices in κ's phase. Alternatively, in the case where the charged lepton sector has $\mathcal{M}_l$ of the form given

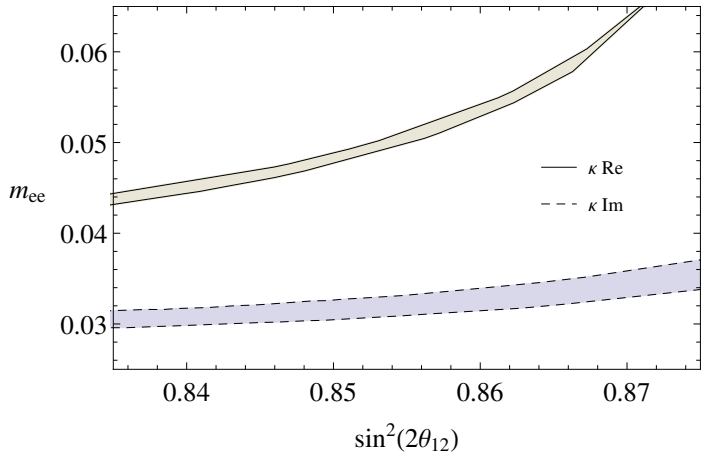

Figure 3.10: Predictions of m_{ee} versus $\sin^2(2\theta_{12})$ for $\sin^2(2\theta_{13}) = 0.095 \pm 0.0105$.

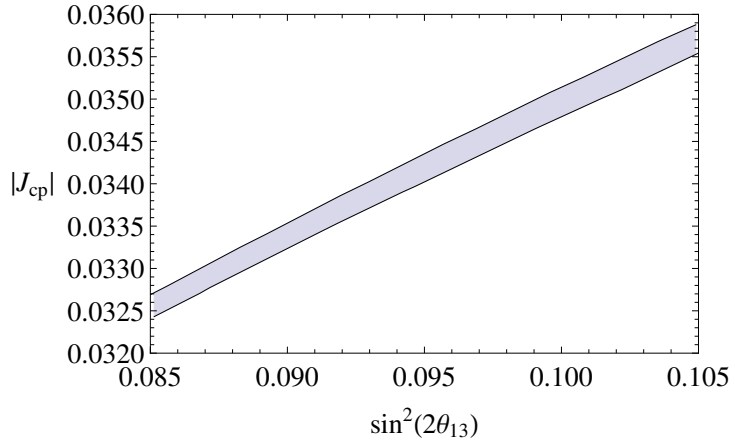

Figure 3.11: Predictions of J_{CP} versus $\sin^2(2\theta_{13})$ for κ imaginary and $\sin^2(2\theta_{12}) = 0.857 \pm 0.025$.

by Eq. 3.51 then to get to the tribimaximal basis it is necessary to transform $\mathcal{M}_\nu$ from Eq. 3.46 such that

$$\mathcal{M}_\nu = U2 \begin{pmatrix} a + f(b+c)/2 & (b+c)/\sqrt{2} & f(-b+c)/2 \\ (b+c)/\sqrt{2} & fa & (b-c)/\sqrt{2} \\ f(-b+c)/2 & (b-c)/\sqrt{2} & a - f(b+c)/2 \end{pmatrix} U2^{\mathrm{T}}, \tag{3.75}$$

where

$$U2 = \begin{pmatrix} 0 & 1 & 0 \\ 1/\sqrt{2} & 0 & -i/\sqrt{2} \\ 1/\sqrt{2} & 0 & i/\sqrt{2} \end{pmatrix}, \tag{3.76}$$

where $U_{TBM} = U_\omega^\dagger U_2$. Note that in this form there is an additional phase of the form that $e^{i2\alpha} = -1$; to return to the form of Eq. 3.46 it is necessary to rotate away this additional phase. Re-writing these parameters in an analogous way as in the case when $\mathcal{M}_l$ is diagonal using $f = -1 + \epsilon'$, $\eta' = (b+c)/2a$, and $\kappa' = (b-c)/2a$, yields

$$\mathcal{M}_\nu^{\mathrm{TB}} \approx \begin{pmatrix} 1-\eta' & \sqrt{2}\eta' & \sqrt{2}\kappa' \\ \sqrt{2}\eta' & -1+\epsilon' & \kappa' \\ \sqrt{2}\kappa' & \kappa' & 1+\eta' \end{pmatrix} a, \tag{3.77}$$

where ϵ', η', κ' are assumed to be small compared to one as before. Incidentally, this yields the same approximate solution as the case when $\mathcal{M}_l$ is diagonal after the following substitutions are made:

$$a = \frac{-3b}{2}, \quad \eta' = \frac{\zeta}{6}, \quad \kappa' = \frac{\kappa}{2\sqrt{6}}, \quad \epsilon' = \frac{-4\epsilon}{3}. \tag{3.78}$$

Additionally, the predicted value of m_{ee} is approximately identical, and thus the numerical predictions of this second model are largely indistinguishable from the first model even after dispensing with the approximation.

3.4 Scotogenic Model with $\mu - \tau$ Interchange Symmetry

In 2002 a special form of the neutrino mass matrix first appeared appeared in Refs. [66, 88], and can be written as:

$$\mathcal{M}_\nu = \begin{pmatrix} A & C & C^* \\ C & D^* & B \\ C^* & B & D \end{pmatrix}, \tag{3.79}$$

where, A and B are real. As discussed in Refs. [6, 72], this neutrino mass matrix can be implemented utilizing a discrete Z_3 flavor symmetry. Additionally, the pattern for the mass matrix in 3.79 has been shown [87] to be protected by an interchange symmetry (that is e $\rightarrow$ e and $\mu \leftrightarrow \tau$) along with CP conjugation. This pattern of mixing matrix is of continued interested because it allows $\theta_{13} \neq 0$ while θ_{23} and δ_{CP} are maximal [6]; these predictions and the interchange symmetry are consistent with the present experimental data. In the analysis of Ref. [72], the ratio of the Yukawa couplings $\lambda = f_\tau / f_\mu$ was taken to be 1 though this assumption can be relaxed as shown in Ref. [6]:

$$\mathcal{M}_\nu^\lambda = \begin{pmatrix} 1 & 0 & 0 \\ 0 & 1 & 0 \\ 0 & 0 & \lambda \end{pmatrix} \mathcal{M}_\nu \begin{pmatrix} 1 & 0 & 0 \\ 0 & 1 & 0 \\ 0 & 0 & \lambda \end{pmatrix}. \tag{3.80}$$

Instead of the simplest scotogenic model, the model in Ref. [6] utilizes an earlier proposal of one-loop generated neutrino mass from Ref. [89] and analyzed in Ref. [72]. The mechanism, seen in Fig. 3.12 generates an inverse seesaw mass as discussed in Refs. [6, 72] and has three additional scalar singlets, $s_{1,2,3}$, a Dirac fermion doublet (E^0, E^-) and a Dirac fermion singlet N. All of the additional particles are odd under an exactly conserved Z_2 symmetry, and the lightest neutral particle is a DM candidate. The neutral components of the doublet mix with the singlet via the SM Higgs, in addition to invariant Dirac masses m_E and m_N.

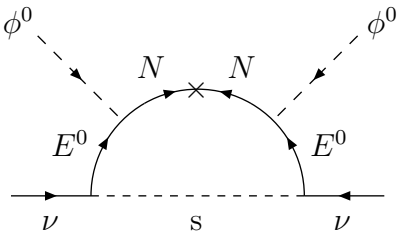

Figure 3.12: One-loop generation of inverse seesaw neutrino mass.

After the Higgs gains a VEV, this results in a mass matrix that connects $(\bar{N}_L, \bar{E}^0_L)$ and (N_R, E^0_R):

$$\mathcal{M}_{N,E} = \begin{pmatrix} m_N & m_D \\ m_F & m_E \end{pmatrix}, \tag{3.81}$$

which results in two Dirac fermions of masses $m_{1,2}$ that are a mixture of N and E^0. Additionally, N has a Majorana mass given by $\frac{m_R}{2} N^c_R \bar{N}_R + \frac{m_L}{2} N^c_L \bar{N}_L$. To diagonalize the mass matrix in 3.81 the left-handed components need to be rotated separately from the right-handed, in an analogy to the SM lepton sector:

$$\mathcal{M}_{1,2} = \begin{pmatrix} m_1 & 0 \\ 0 & m_2 \end{pmatrix} = U_L^T \begin{pmatrix} m_N & m_D \\ m_F & m_E \end{pmatrix} U_R, \tag{3.82}$$

where the matrices U_L and U_R can be parameterized as rotation matrices:

$$U_{R,L} = \begin{pmatrix} \cos\theta_{R,L} & -\sin\theta_{R,L} \\ \sin\theta_{R,L} & \cos\theta_{R,L} \end{pmatrix}, \tag{3.83}$$

with the mixing angles

$$m_D m_E + m_F m_N = \sin(\theta_L)\cos(\theta_L)(m_1^2 - m_2^2) \tag{3.84}$$

$$m_D m_N + m_F m_E = \sin(\theta_R)\cos(\theta_R)(m_1^2 - m_2^2). \tag{3.85}$$

Using these mixing angles, the E and N states can be written in terms of the mass eigenstates ω_1 and ω_2

$$\begin{pmatrix} N_{(R,L)} \\ E_{(R,L)} \end{pmatrix} = \begin{pmatrix} \cos\theta_{(R,L)} & \sin\theta_{(R,L)} \\ -\sin\theta_{(R,L)} & \cos\theta_{(R,L)} \end{pmatrix} \begin{pmatrix} \omega^1_{(R,L)} \\ \omega^2_{(R,L)} \end{pmatrix}. \tag{3.86}$$

The loop in Fig. 3.12 can be calculated after inserting the Majorana masses m_R and m_L and using the Yukawa interaction $fs\bar{E}^0_R\nu_L$, however it is convenient to first split the calculation into sub-diagrams using the proper combinations of ω_1 and ω_2 from Eq. 3.86, and finding the full mass term by summing over each possible combination. In order to illustrate how this can be done, consider the representation of these sub-diagrams coming from the m_R and m_L mass insertions respectively in Fig. 3.13. After taking into account the proper

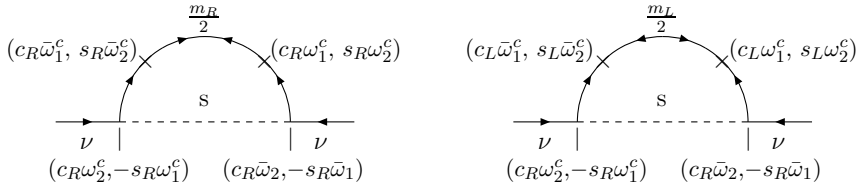

Figure 3.13: The scotogenic one-loop mechanism, written using the mass eigenstates with Majorana mass insertions to complete the loop.

combinations of chirality — see Appendix B — the neutrino mass can be calculated:

$$\begin{aligned} m_\nu = {} & f^2 m_R \cos^2\theta_R \sin^2\theta_R (m_1^2 - m_2^2)^2 \int \frac{d^4k}{(2\pi)^4} \frac{k^2}{k^2 - m_s^2} \frac{1}{(k^2 - m1^2)^2} \frac{1}{(k^2 - m2^2)^2} \\ & + f^2 m_L m_1^2 \cos^2\theta_R \sin^2\theta_L \int \frac{d^4k}{(2\pi)^4} \frac{1}{k^2 - m_s^2} \frac{1}{(k^2 - m1^1)^2} \\ & + f^2 m_L m_2^2 \sin^2\theta_R \cos^2\theta_L \int \frac{d^4k}{(2\pi)^4} \frac{1}{k^2 - m_s^2} \frac{1}{(k^2 - m2^2)^2} \\ & - 2f^2 m_L m_1 m_2 \cos\theta_R \sin\theta_R \cos\theta_L \sin\theta_L \int \frac{d^4k}{(2\pi)^4} \frac{1}{k^2 - m_s^2} \frac{1}{k^2 - m1^2} \frac{1}{k^2 - m2^2} \end{aligned} \tag{3.87}$$

In general, the diagonalized 3x3 neutrino mass matrix $\mathcal{M}_d$ defined as

$$\begin{pmatrix} m_1 & 0 & 0 \\ 0 & m_2 & 0 \\ 0 & 0 & m_3 \end{pmatrix}, \tag{3.88}$$

where $m_{(1,2,3)}$ are the physical neutrino masses, is found from the non-diagonal mass matrix $\mathcal{M}_\nu$ via

$$\mathcal{M}_d = E_\alpha U^{\mathrm{T}} E_\beta \mathcal{M}_\nu E_\beta U E_\alpha, \tag{3.89}$$

where

$$E_{\alpha,\beta} = \begin{pmatrix} e^{i(\alpha,\beta)_1} & 0 & 0 \\ 0 & e^{i(\alpha,\beta)_2} & 0 \\ 0 & 0 & e^{i(\alpha,\beta)_3} \end{pmatrix}. \tag{3.90}$$

While there are six phases in Eq. 3.89, only three of the phases are physical — two relative Majorana phases and one Dirac phase [10]. The differences in neutrino masses squared are the relevant parameters for neutrino oscillation data:

$$\mathcal{M}_d^2 = E_\alpha^\dagger U^\dagger \mathcal{M}_\nu (\mathcal{M}_\nu)^\dagger U E_\alpha \tag{3.91}$$

This general procedure also works for the mass matrix from Ref. [72]. Using Eq. 3.80 it is possible to relate the solutions of Ref. [72] to the more general case where $\lambda \neq 1$ in Ref. [6]. Applying Eq. 3.80 to the diagonalized mass matrix yields

$$\begin{pmatrix} 1 & 0 & 0 \\ 0 & 1 & 0 \\ 0 & 0 & \lambda \end{pmatrix} \mathcal{M}_d^2 \begin{pmatrix} 1 & 0 & 0 \\ 0 & 1 & 0 \\ 0 & 0 & \lambda \end{pmatrix} = \begin{pmatrix} m_1^2 & 0 & 0 \\ 0 & m_2^2 & 0 \\ 0 & 0 & \lambda^2 m_3^2 \end{pmatrix} = \mathcal{M}_{\lambda d}^2. \tag{3.92}$$

Applying Eq. 3.80 to Eq. 3.91 results in

$$\mathcal{M}^2_{\lambda d} = E^\dagger_\alpha \begin{pmatrix} 1 & 0 & 0 \\ 0 & 1 & 0 \\ 0 & 0 & \lambda \end{pmatrix} U^\dagger \mathcal{M}_\nu (\mathcal{M}_\nu)^\dagger U \begin{pmatrix} 1 & 0 & 0 \\ 0 & 1 & 0 \\ 0 & 0 & \lambda \end{pmatrix} E_\alpha. \tag{3.93}$$

Defining a new matrix Δ such that

$$\Delta = U^\dagger \begin{pmatrix} 0 & 0 & 0 \\ 0 & 0 & 0 \\ 0 & 0 & (\lambda - 1) \end{pmatrix} U, \tag{3.94}$$

allows us to simplify Eq. 3.93 so it is entirely in terms of the mass matrices where $\lambda \neq 1$:

$$\mathcal{M}^2_{\lambda d} = E^\dagger_\alpha U^\dagger (1 + \Delta^\dagger) \mathcal{M}^\lambda_\nu (\mathcal{M}^\lambda_\nu)^\dagger (1 + \Delta) U E_\alpha \tag{3.95}$$

To find the physical neutrino masses $\mathcal{M}^2_{\lambda d}$ must be diagonalized using an additional orthogonal matrix, which can be found numerically via

$$(1 + \Delta)\mathcal{M}^2_{\lambda d}(1 + \Delta)^\dagger = O \mathcal{M}^2_{\text{phys}} O^{\text{T}}, \tag{3.96}$$

where $\mathcal{M}^2_{\text{phys}}$ is the diagonal matrix of the physical neutrino masses. Note that the masses in $\mathcal{M}^2_{\lambda d}$ are those used in the case that $\lambda = 1$, and U is the resulting PMNS matrix with $\theta_{23} = \pi/4$ and $\delta = \pm\pi/2$ as described in Ref. [72]. These values can be related by solving

$$A O \mathcal{M}^2_{\text{phys}} O^{\text{T}} A^\dagger, \tag{3.97}$$

where $A = (1 + \Delta)^{-1}$. A is entirely fixed by the choice in λ, and O has three parameters which can be found, after the physical masses are fixed, using the constraint that the off-diagonals in $\mathcal{M}^2_{\lambda d}$ must be zero. Once the parameters for O are found, the full mixing

matrix is given by UO from which the correlation of θ_{23} and δ_{CP} are extracted [6]. There is an ambiguity in the choice of the physical masses, as only $|\Delta m^2_{32}|$ and Δm^2_{21} are known, and the remaining mixing angles are varied to produce the correct experimental limits. For the analysis in Ref. [6], the 2014 PDG values [10] were used:

$$\sin^2(2\theta_{12}) = 0.846 \pm 0.021,\ \Delta m^2_{21} = (7.53 \pm 0.18) \times 10^{-5}\text{eV}^2,$$

$$\sin^2(2\theta_{23}) = 0.999\ {}^{+0.001}_{-0.018},\ \Delta m^2_{32} = (2.44 \pm 0.06) \times 10^{-3}\text{eV}^2 \text{ (normal hierarchy)},$$

$$\sin^2(2\theta_{23}) = 1.000\ {}^{+0.000}_{-0.017},\ \Delta m^2_{32} = -(2.52 \pm 0.07) \times 10^{-3}\text{eV}^2 \text{ (inverted hierarchy)}.$$

$$\sin^2(2\theta_{13}) = (9.3 \pm 0.8) \times 10^{-2}.$$

As discussed in Ref. [6], there are similar constraints on δ_{CP} and θ_{23} when looking at normal and inverted hierarchy solutions, so there is an insensitivity to mass hierarchy in the predictions of the model for $\lambda \neq 1$. Both normal and inverted hierarchies are considered with $m_{1,3} = 0, 0.03, 0.06$ eV and $\lambda > 1$, after which θ_{13} and θ_{12} in U are varied and AO is determined numerically to produce $\mathcal{M}^2_{\lambda d}$ to determine the full mixing matrix given by UO. Solutions are fixed by choosing central values of $\Delta m_2 1^2$, $\Delta m_3 2^2$, $\sin^2(2\theta_{12})$, and $\sin^2(2\theta_{13})$. In Figs. 3.14 and 3.15 $\sin^2(2\theta_{23}$ and δ_{CP} are plotted versus λ. As seen in Fig 3.14 $\lambda < 1.15$ is required in order to maintain $\sin^2(2\theta_{23}) > 0.98$. Additionally, δ_{CP} is insensitive to variations in m_1 and $\delta_{CP} > 0.95\pi/2$ is required to satisfy $\sin^2(2\theta_{23}) > 0.98$. As discussed in Ref. [6] for the case that $\lambda > 1$ it was numerically determined that $\theta_{23} < \pi/4$. Similar results are seen for the inverted hierarchy case in Figs. 3.19 and 3.20. The case for $\lambda < 1$ is equivalent to $\lambda^{-1} > 1$ with a $\mu - \tau$ exchange, and results for $\lambda > 1$ can be mapped to $\lambda < 1$ using $\lambda \to \lambda^{-1}$ as illustrated in Figs. 3.17 and 3.18. In the mass scheme considered here and in Ref. [6], the neutrinoless double beta decay parameter m_{ee} is very close to m_1 for normal hierarchy and $m_3 + \sqrt{\Delta m^2_{32}}$ for an inverted hierarchy. The results are summarized in Figs.

3.16 and 3.21 for normal and inverted mass-hierarchy respectively.

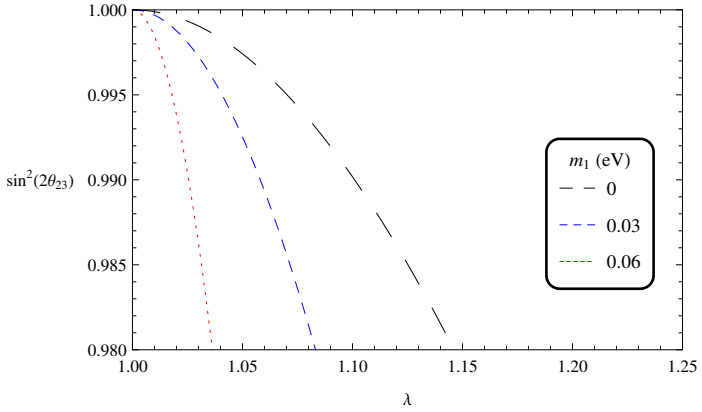

Figure 3.14: $\sin^2(2\theta_{23})$ versus λ for a normal mass-hierarchy.

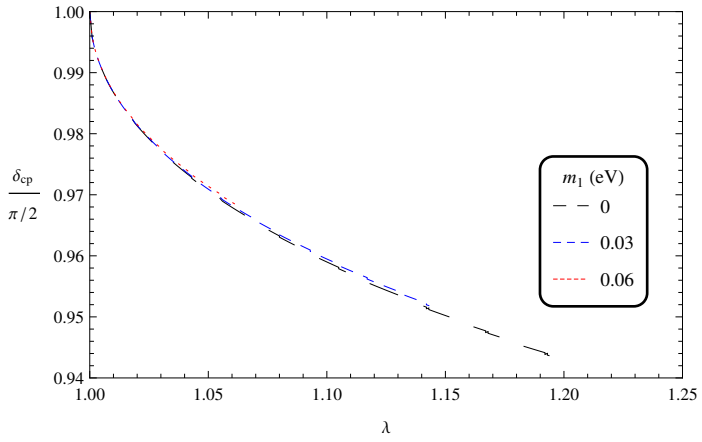

Figure 3.15: The Dirac CP violating phase (δ_{CP}) versus λ for a normal mass-hierarchy.

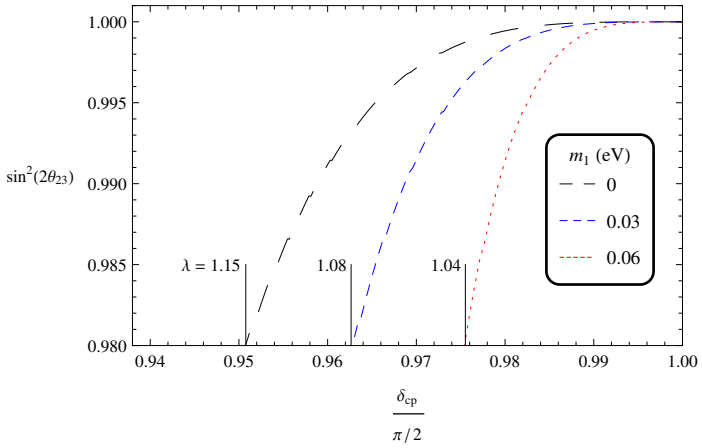

Figure 3.16: $\sin^2(2\theta_{23})$ versus δ_{CP} for a normal mass-hierarchy.

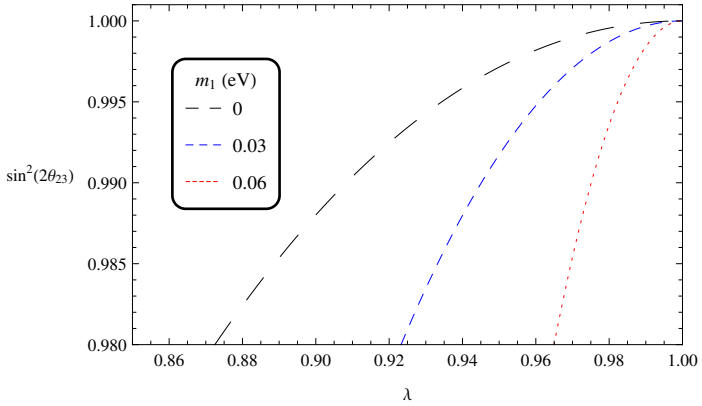

Figure 3.17: $\sin^2(2\theta_{23})$ versus λ for $\lambda < 1$ and normal hierarchy, demonstrating the mapping of $\lambda \to \lambda^{-1}$.

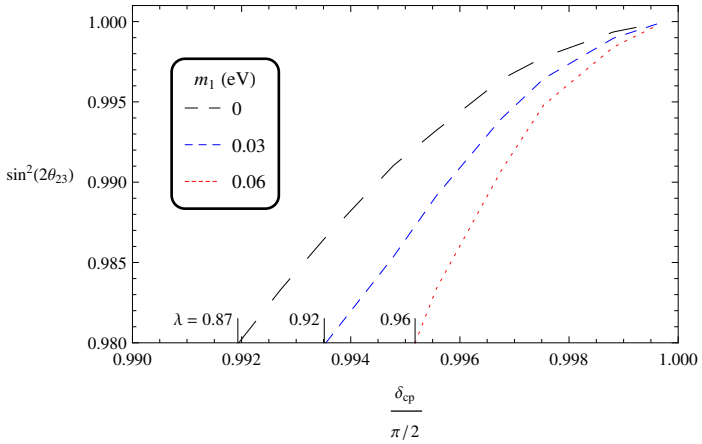

Figure 3.18: $\sin^2(2\theta_{23})$ versus δ_{CP} for $\lambda < 1$ and normal hierarchy, demonstrating the mapping of $\lambda \to \lambda^{-1}$.

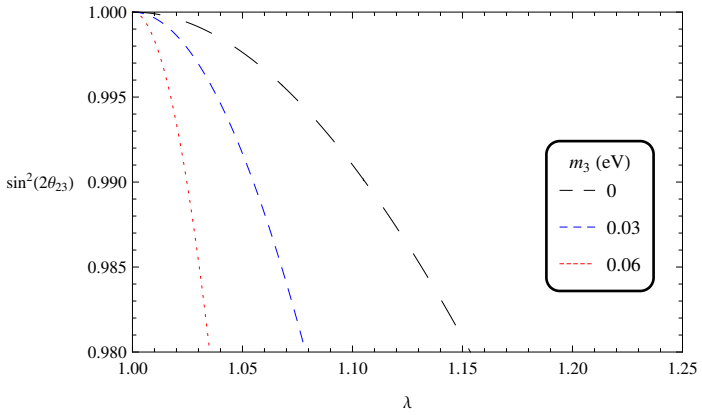

Figure 3.19: $\sin^2(2\theta_{23})$ versus λ for an inverted mass-hierarchy.

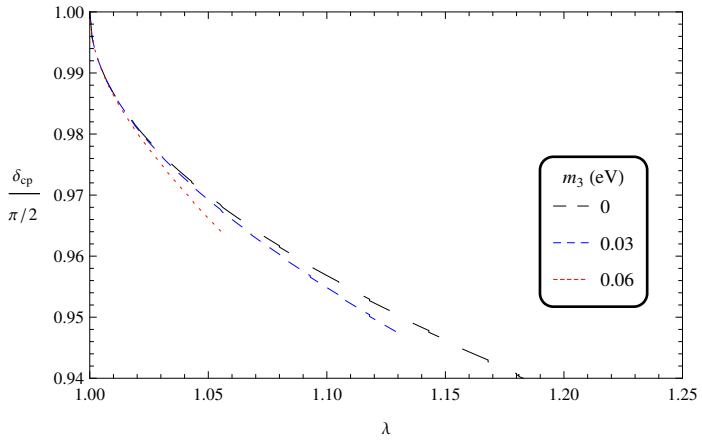

Figure 3.20: The Dirac CP violating phase (δ_{CP}) versus λ for an inverted mass-hierarchy.

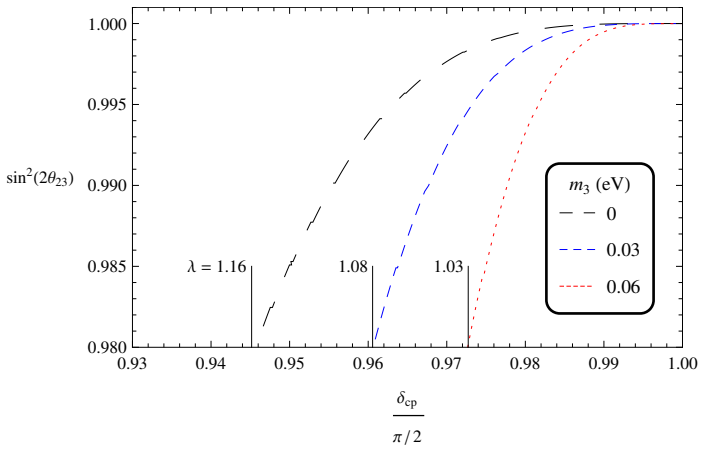

Figure 3.21: $\sin^2(2\theta_{23})$ versus δ_{CP} for an inverted mass-hierarchy.

Chapter 4

Collider Phenomenology

4.1 Introduction

For many processes at colliders, calculating the theoretical cross section (for either signal or background events), is in principle a straight forward and familiar process. After deriving the Feynman rules from a given Lagrangian, invariant amplitudes are calculated and squared, spins or external polarizations are summed, and the phase space integral is calculated. However, in an actual experiment, there are several complicating factors:

1. The resulting calculation doesn't represent the effects of statistical fluctuations and finite sample sizes.

2. Phase space integrals, particularly for many-body processes, can be tedious and complicated.

3. Initial states may have indefinite initial momentum or a distribution of many states (e.g. in the case of proton or nucleon accelerators).

4. Many diagrams may be required to be calculated and summed over.

5. Low-energy QCD effects may complicate both initial and final states.

Additionally, as measurements of physical processes become more precise, increasingly realistic simulations are sought after to determine what new physics signatures may look like inside an actual particle detector. Because of these factors, it is necessary (or practical) to utilize automation. Automated Monte Carlo methods are utilized in order to calculate phase space integrals, simulate the effects of finite sample size, and more realistically simulate detector response. For a comprehensive review of Monte Carlo methods in particle physics and for the basic designs of Monte Carlo event generators see Ref. [10].

4.1.1 Programs, Tools, and Methods

In order to quickly and more realistically analyze collider signatures originating in novel physics, it is important to first implement the model in a parton-level event generator such as Madgraph [90] or CalcHEP [91]. These patron-level event generators take into account the complicated initial states for proton-proton colliders such as the LHC, and use Monte Carlo methods and Parton Distribution Functions (PDFs) to produce lists of events for a process of interest. These event lists are often produced in the Les Houche Event format and list initial, intermediate, and final state particle energy and momentum among other physically measured properties and particle identification codes. The final states in these event lists are parton-level states, that is the process of hadronization isn't taken into account at this level and quarks and gluons are left as free particles. These events can then be passed on to a more sophisticated event generator such as PYTHIA [92, 93] which simulates the low-energy QCD processes and allows a simulation of hadronization, QED showers, etc. It is also possible to implement various kinematic cuts in PYTHIA to take into account the pseudorapditiy inside a detector and also and can implement algorithms such as FastJET [94] to identify jets of particles that had a common origin (such as a free quark that hadronized). After the patron-level events are hadronized, it is also possible to continue with the simulation and pass these events to various programs that simulate the particular detectors response to these particles, increasing the realism of the simulated new physics signal. For the purposes of the collider signature analysis in this thesis the

simulation provided by PYTHIA has been considered adequate in determining whether or not a model may be able to yield a clear signal at the LHC, and the details of the specific programs implemented and which settings were used are discussed in the sections below.

4.2 Scotogenic Model, A_4, with WDM

In the minimal scotogenic model, a general relationship for the loop-generation of neutrino mass was obtained [32]. In section 3.2, the analysis of a particular assumption of the scalar and fermion masses was discussed, but it is also possible to take a different limit (see Appendix A). If the dark scalar doublet has a large mass, then it is the neutral fermions (N) that act as a dark matter candidate and the resulting neutrino mass matrix gives a inverse seesaw like mass matrix (see Eq. A.7 from Appendix A):

$$(\mathcal{M})_{ij} = \frac{ln(m_R^2/m_I^2)}{16\pi^2} \sum_k h_{ik} h_{jk} M_k. \tag{4.1}$$

In order to explain the smallness of the neutrino mass the masses of the additional fermions N are large, however for this expression either the Yukawa coupling is required to be tuned to be extremely small, or the mass of N is much smaller than the electroweak scale. Alternatively, if the mass splitting between the real and imaginary components of η is small, then the mass is suppressed by the log term, but this isn't strictly necessary, and for a splitting of 110 GeV this term is close to 1 ($\log(m_R^2/m_I^2 = 0.94)$. If the new neutral fermions are assigned a lepton number $L = -1$, then L is conserved in all interactions except the Majorana mass term which violates lepton number by two units, but continue to conserve $(-1)^L$. As this mass term is taken to zero, the lepton violation term is eliminated, and fully conserved lepton number is restored, thus the smallness of the N mass is natural. Moreover, it can be argued that this mass should be on the order of the electron mass, which is the smallest lepton conserving mass. With $M_{N_k} \sim 10$ keV and $h^2 \sim 10^{-3}$, then $m_\nu \sin 0.1$ eV. With m_η on the order of 10^2 GeV, then N can be considered "sterile" making it a warm

dark matter (WDM) candidate dubbed the scotino [95, 96]. Many models of WDM have various constraints from astrophysical observation [97, 98], in particular a popular model of WDM are the sterile neutrinos, which are reviewed in Ref. [99]. However, the lightest scotino is absolutely stable and does not mix with the neutrinos and does not contribute to galactic x-ray emissions avoiding the upper bound of 2.2 keV on WDM mass [97]. The Lyman-α forest observations still apply to the scotino and yield a lower bound of around 5.6 keV [98].

Because the scotino is light, it potentially contributes to muon decay, flavor changing neutral currents ($\mu \to e\gamma$), and the muon anomalous magnetic moment. However, with the addition of an A_4 flavor symmetry the contributions to these terms, as well as the phenomenology of the scotino and the dark scalar doublet, can be significantly changed. Consider the case where the doublet η is a singlet under A_4 and $(\nu_i, l_i), N_k \sim \mathbf{3}$, then the Yukawa couplings in Eq. 4.1 become

$$h_{ik} = h\delta_{ik}, \tag{4.2}$$

and the neutrino mass matrix is simply

$$\mathcal{M}_\nu = \zeta \mathcal{M}_N, \tag{4.3}$$

where $\zeta = h^2 \frac{\log(m_R^2/m_I^2)}{16\pi^2}$. The A_4 flavor symmetry may be replaced by any flavor symmetry as long as Eq. 4.2 is possible using singlet and triplet representations of the flavor symmetry. Since the interactions with N_k and the charged leptons occur through η^+ and depend on the Yukawa couplings h_{ik} and the PMNS matrix elements $U_{l\nu}$, the flavor-changing neutral current of $\mu \to e\gamma$ is highly suppressed — the leading term is proportional to $\sum_k h_{\mu k} h^*_{ek}$, which is equal to $|h|^2 \sum_k U_{\mu k} U^*_{ek}$ and is exactly zero. The next-to-leading term is non-zero but is negligibly small, and so there is no useful bound on η^+ from muon decay. The scotino also potentially changes the SM muon anomalous moment Δa_μ, and this contribution has

been calculated in Ref. [100]:

$$\Delta a_\mu = \sum_k \frac{h_{k\mu}^2 m_\mu^2}{(4\pi)^2 m_\eta^2} F_2(s_{N_k}), \tag{4.4}$$

where $s_{N_k} = m_{N_k}^2/m_\eta^2$, and

$$F_2(x) = \frac{1 - 6x + 3x^2 + 2x^3 - 6x^2 \log x}{6(1-x)^4} \tag{4.5}$$

(see Ref. [100] for details). Unlike the case presented in Ref. [100], if η is in the hundred GeV mass range and the scotinos are in the keV mass range then the model in Ref. [3] has a small s_{N_K}, and thus Eq. 4.5 at leading order becomes

$$F_2(x) \approx 1/6, \tag{4.6}$$

and Eq. 4.4 is thus

$$\Delta a_\mu = \sum_k \frac{h_{k\mu}^2 m_\mu^2}{96\pi^2 m_\eta^2}. \tag{4.7}$$

And given Eq. 4.2, this yields the total contribution to the Δa_μ of the form

$$\Delta a_\mu = -\frac{m_\mu^2 |h|^2}{96\pi^2 m_\eta^2} = -1.18 \times 10^{-12} \left(\frac{|h|^2}{10^{-3}}\right) \left(\frac{100 \text{ GeV}}{m_\eta}\right)^2, \tag{4.8}$$

and so the contribution to the SM is negligible. While the lightest scotino is absolutely stable there are three, and the heavier scotinos decay vis $N_3 \to N_1 \bar{\nu}_1 \nu_3$, where N_1 is the lightest scotino and $N_{2,3}$ are the heavier states. This decay rate occurs through $\eta_{R,I}$ and is given by

$$\begin{aligned} \Gamma(N_3 \to N_1 \bar{\nu}_1 \nu_3) = {} & \frac{|h|^4}{256\pi^3 M_{N_3}} \left(\frac{1}{m_R^2} + \frac{1}{m_I^2}\right)^2 \\ & \times \left(\frac{M_{N_3}^6}{96} - \frac{M_{N_1}^2 M_{N_3}^4}{12} - \frac{M_{N_1}^8}{96 M_{N_3}^2} + \frac{M_{N_1}^4 M_{N_3}^2}{8} \log \frac{M_{N_3}^2}{M_{N_1}^2}\right), \end{aligned} \tag{4.9}$$

If $M_{N_1} = 10$ keV, $M_{N_3} = 14.85$ keV, $|h|^2 = 10^{-3}$, $m_R = 240$ GeV, and $m_I = 150$ GeV then this decay rate is 1.0×10^{-46} GeV which yields a lifetime of 2.1×10^{14} years that is much larger than the age of the universe. The lifetime of N_2 is even longer as the differences in mass-squared for neutrinos are related to the mass-squared differences between the scotinos and $\Delta m^2_{21} \ll \Delta m^2_{31}$. As a result N_2 and N_3 are stable enough to contribute to the observable DM, but this doesn't yield an appreciable contribution to x-ray signatures via $N_{2,3} \to N_1\gamma$ for the same reasons that $\mu \to e\gamma$ is suppressed, namely the A_4 flavor symmetry prevents the leading order term which significantly reduces galactic x-ray signatures. Because the scotinos are of order of 10s of keV, muon decay can occur at tree level through $\mu \to N_\mu e\bar{N}_e$, giving the inclusive rate of

$$\Gamma(\mu \to N_\mu e\bar{N}_e) = \frac{|h|^4 m_\mu^5}{6144\pi^3 m_\eta^4}. \tag{4.10}$$

The muon decay through scotinos potentially changes the experimental measurement of the Fermi constant G_F, which leads to a lower bound on the charged η mass of

$$m_{\eta^+} > 70 \text{ GeV}. \tag{4.11}$$

Additionally, there are existing bounds on the charged η mass from LEP that yield a lower mass range between 70 to 90 GeV [101]. This mass range prevents the 125 GeV Higgs from decaying directly to pairs of charged η, however the dark scalars do contribute to the $H \to \gamma\gamma$ rate as discussed in the Refs. [102–105]. In earlier LHC runs, the Higgs decay to two photons had an intriguing excess [106] whereas the current data shows this rate to be largely consistent with the SM prediction [107], potentially further constraining the $\eta^\pm$ mass. For the analysis presented here and in Ref. [3] has not been taken these new constraints into account. A novel prediction of this model is the Yukawa coupling between η, N, and the charged leptons occurs with equal strength to each generation of charged lepton. Additionally, because of the A_4 flavor symmetry and the assignment of leptons and

scotinos as A_4 triplets, the decays are

$$\eta^{\pm} \to e^{\pm} N_1, \mu^{\pm} N_2. \tag{4.12}$$

If the mass of η is low enough then it is possible for the charged dark scalar to be pair produced at the LHC. The structure of the Yukawa sector restricts the decay of η into pairs of charged leptons with $e^+\mu^-$ or $e^-\mu^+$ 1/9 of the time along with large missing energy from the scotinos. Such signatures also can occur from W^+W^- production, with subsequent decays to leptons and a neutrino. To analyze the model in Ref. [3], the model is implemented in CalcHEP [91] to generate parton-level events using the CTEQ6L [108] parton distribution functions which are then analyzed by PYTHIA [92] to produce leading-order (LO) results for the signal events coming from η pair production. The background events coming from W pair production were produced using PYTHIA [92] and were scaled to the next-to leading-order cross-section for W^+W^- at the 8 TeV LHC (57.3 pb). To analyze both the background and the signal, basic cuts to transverse momentum and pseudorapidity ($p_T > 10$ GeV and $|\eta| < 2.5$) are applied to the leptons in the final state. A variety of additional transverse momentum cuts were applied to the leptons, in addition to cuts on the missing transverse energy, in an attempt to find a set of cuts that reduce the SM background below that of the signal. While scanning over combinations of cuts, it was found that the most relevant parameter for signal/background discrimination is the missing energy, and the results of several missing energy cuts using a variety of $m_{\eta^{\pm}}$ are summarized in Table 4.1. After these cuts are applied, the SM background signal can be significantly reduced from its initial value of 57.3 pb down to as low as 8.6 fb, however since the initial cross-section for η pair-production is on the order of 10^2 fb no cuts were found that allowed the signal to exceed the background [3]. As discussed in Ref. [3], it is possible to increase the scotogenic particle content to complete SU(5) multiplets which is discussed further in Ref. [109] and a case where complete multiplets are used (without gauge coupling unification) is demonstrated

$m_{\eta^\pm}$ (GeV)	σ (fb) for various $E_{\mathrm{T}}^{\mathrm{miss}}$ cuts:	0 GeV	25 GeV	50 GeV	100 GeV
80		33.2	27.9	18.3	2.88
90		22.7	19.8	14.4	3.10
100		15.7	14.0	10.6	3.08
110		11.4	10.3	8.13	3.03
120		8.72	7.99	6.54	2.91
130		6.45	5.98	5.05	2.57
140		4.97	4.64	3.96	2.21
150		3.84	3.62	3.16	1.89
	SM Background σ (fb):	626	453	206	8.60

Table 4.1: Cuts applied to the signal and background for opposite-sign opposite-flavor dileptons + missing energy (E_T^{miss}).

in Ref. [5] and is discussed in Section 4.3. This SU(5) completion makes it possible to have strongly produced scalars which may be potentially seen at future LHC runs.

4.3 Strong Production in Scotogenic Model

As pointed out in Section 2.3.4, it is possible to extend the scotogenic model to generate quark and lepton masses [73], by forbidding the tree-level Yukawa couplings of the lightest generation of quarks and leptons via any non-Abelian discrete flavor symmetry [5]. Additionally, these new particles allow the scotogenic model to have complete SU(5) multiplets, which can be extended to form a GUT in a non-minimal model as described in Section 2.3.4. Since the model connects DM and quark and lepton masses through a single SM Higgs boson the problems with earlier flavor symmetry models (namely the need for many new scalars) is avoided. As discussed in Ref. [33], the new Yukawa coupling constants can potentially deviate from the SM prediction and are either larger or smaller than the SM value. The analysis in this thesis follows that of Ref. [5], however many of the generic predictions are similar to the model found in Ref. [73] but are worked out in detail and analyzed with CalcHEP [91], Madgraph [90], and PYTHIA [93].

Just as in the minimal scotogenic model there is an additional Z_2 symmetry, under which all additional particles to the SM are odd. In this case, this serves a similar function

to R-parity in SUSY. The additional particles allow for the modified scotogenic mechanism illustrated in Fig. 2.2, and their transformations under the SM gauge group are summarized in Table 4.2. In this model, the flavor symmetry is carried by the neutral fermions N — the

Field	Spin	$SU(3)_C$	$SU(2)_L$
(η^+, η^0)	0	1	2
χ^+	0	1	1
$(\xi^{2/3}, \xi^{-1/3})$	0	3	2
$\zeta^{2/3}$ $\zeta^{-1/3}$	0	3	1
$N_{1,2,3}$	1/2	1	1

Table 4.2: Relevant particle content for unified quark and lepton mass scotogenic mechanism.

DM candidates of the model — which is softly broken by the mass matrix $\mathcal{M}_N$. This flavor symmetry also forbids the usual tree-level Yukawa terms for the quarks and leptons, and for a suitable choice of flavor symmetry can be utilized so that the first two generations have radiative mass, while the top and bottom quarks could still have tree-level masses. The new color-triplet fields are analogous to the squarks from SUSY, with the exception that these new scalars do not have family structure and do not carry flavor. The flavor information is carried by the Dirac fermions N. Since these new fields are color-triplets they can be pair-produced directly at the LHC via gluons (see Fig. 4.1). This is a notable difference

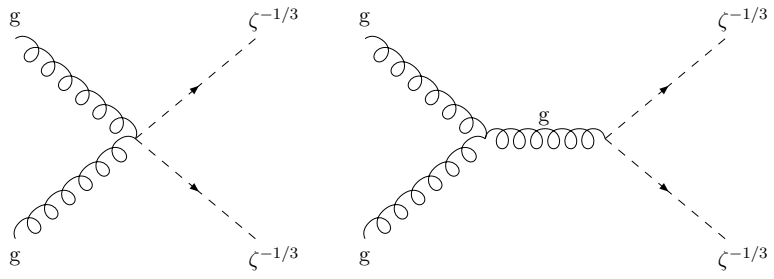

Figure 4.1: Feynman diagrams for squark pair-production.

from the previous scotogenic model in Section 4.2, in which the main particles of interest

were produced electroweakly. While the flavor structure is fixed by the chosen symmetry, a specific pattern for the Yukawa couplings has been assumed [5]:

$$\mathcal{L} = f(\bar{d}_R N_{1L} + \bar{s}_R N_{2L})\zeta^{-1/3} + f^{'}(\bar{e}_R N_{1L} + \bar{\mu}_R N_{2L})\chi^{-} + \text{h.c.}, \tag{4.13}$$

where it is also assumed that $m_\zeta > m_{N_2} > m_\chi > m_{N_1}$, so that N_1 is the DM candidate and N_2 decays into N_1 through χ. As mentioned, any of the scalar color-triplets can be pair-produced at the LHC from gluons, and each ζ can decay to a strange quark and a neutral fermion (N_2), or a down quark and a neutral fermion (N_1) due to the Yukawa couplings in Eq. 4.13. Subsequently, any N_2's will decay through χ to $\mu^{\pm}e^{\mp}N_1$. The free quarks (s and d) will hadronize, and be seen as jets in the detector, and N_1 will appears as missing energy (E_T^{miss}). Generically this allows several signatures at the LHC:

1. 2 jets + E_T^{miss}
2. 2 jets + opposite-sign opposite-flavor (OSOF) dileptons + E_T^{miss}
3. 2 jets + four leptons (OSOF) + E_T^{miss}

Since the model above produces several qualitatively distinct signatures, and can be strongly produced, there is a potential for a novel signature at the LHC. As mentioned, the color-triplet ζ behaves as a squark, so it couples to gluons but in the scotogenic model there is no gluino and the squark-analogs do not couple to to quarks except through Eq. 4.13 which always involves $N_{1,2,3}$. As such, the branching fractions of $\zeta \to dN_1$ and $\zeta \to sN_2$ are roughly equal, and are set to 0.5 for the purposes of the analysis here and in Ref. [5]. The mass of the charged scalar χ is constrained to be greater than 70 GeV from LEP data [101]. After analyzing the model with a range of masses, it is found [5] that the best scenarios of optimizing the ratio of the cross sections of the signal divided by background under various cuts are those for $m_{N_2} = 400$ GeV and $m_\chi = 200$ GeV. Thus the choice of the specific mass scheme of $m_\zeta > m_{N_2} > m_\chi > m_{N_1}$, as already mentioned.

To analyze the phenomenology of this model in more detail, the model is imple-

mented in CalcHEP [91] to generate parton-level events using the CTEQ6M PDFs [110], which are then analyzed with PYTHIA 8 [92,93] to produce leading-order (LO) results. The LO production cross section of the squark analogs (hereby referred to simply as squarks) is verified through the Feynrules [111] interface with Madgraph 5 [90], producing a cross section consistent with CalcHEP. Whereas the main signature of this model is distinct from that of SUSY squarks, there are simplified SUSY models with only one light family of squark and the gluinos decoupled (called simplified topologies) which have the same production cross section as the squarks analogs analyzed in this work. Most importantly, the masses excluded by the LHC are much lower for such models as seen in Fig. 4.2. This scenario is used for the expected 13 TeV data where the production cross sections of the squarks are compared to simplified topology models of SUSY squarks, which are calculated at Next-To-Leading-Order (NLO) and Next-Leading-Log (NLL) from Ref. [112]. The comparison of the LO calculation to these results is used to obtain a scale factor in order to approximate the NLO contributions to the squark production by scaling the cross-sections calculated in CalcHEP. For the opposite-sign opposite-flavor dilepton events, the main background is from $t\bar{t}$ pairs. This is different from the case of same-flavor leptons — a generic SUSY signature — which has significant contribution from Drell-Yan production [113]. For the expected 13 TeV data, only the $t\bar{t}$ background is generated with CalcHEP, using a k-factor to scale to the NLO production cross section for $t\bar{t}$ [114], which is then analyzed with PYTHIA 8.

In addition to the opposite-sign opposite-flavor dilepton + 2 jets + E_T^{miss} signature, it is also possible for each squark to decay directly to DM and a quark, thus producing two jets and missing energy, without any lepton. As a result, SUSY searches at 7 TeV and 8 TeV for this signature in simplified SUSY topologies offer useful constraints on the model in Ref. [5]. The searches at 8 TeV [115] are presented in Fig. 4.2. For the current model, the 7 TeV (not shown) and 8 TeV (Fig. 4.2) data are taken into account by ensuring the cross section for ζ decaying directly to dN_1 is lower than the upper limit observed at the LHC for a single squark (in a simplified topology) decaying directly to a quark + LSP. After

these constraints are taken into account, the results from the 7 TeV [116] and 8 TeV [113] searches looking for events with 2 leptons, 2 jets, and missing energy do not provide any further constraints. Additionally, it is possible for the squark to be produced through a

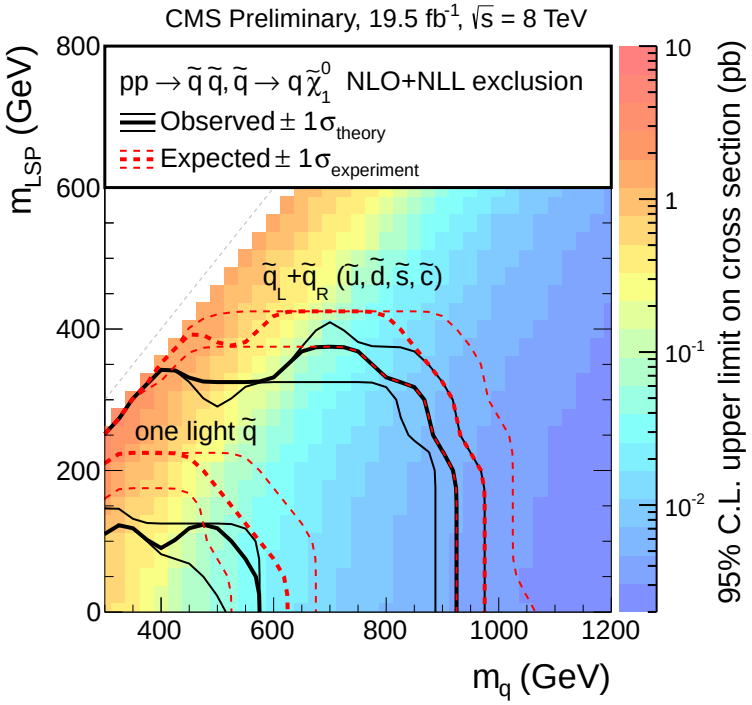

Figure 4.2: Results of squark searches at LHC through quark + LSP at 8 TeV from CMS-PAS-SUS-13-019.

t-channel process directly with DM producing a monojet signal, however this production cross section is a smaller contributor to an LHC signal than the dijet + E_T^{miss}. Such a monojet + E_T^{miss} signature for DM has been investigated in a model independent way (see Refs. [117–120]). When considering the monojet signature, the upper bound of allowed events in the 8 TeV data [118] are taken into account at LO if a squark mass above 400 GeV is assumed. Additionally, studies of DM that can interact with a colored scalar have investigated the constraints from relic abundance and direction detection of DM, which are potentially more restrictive than the LHC [117, 119, 120]. In particular, XENON100 is able to probe down to 10^{-45} cm^2 for a DM mass of 100 GeV [120], which would rule out much

of the parameter space if f is of order unity. However, to yield the proper down quark mass a value of $f \approx 0.01$ must be used and the spin dependent, direct detection, cross section for Dirac fermion dark matter [120] can be of order 10^{-45} cm^2 for a squark mass of 400 GeV and a DM mass of 100 GeV. Calculating the relic density for DM that can interact with quarks via the squark following Ref. [120] yields an incorrect value for $\Omega_{N_1}h^2$ unless $f > 0.5$. Unlike the model in Ref. [120], the scotogenic model has additional contributions to annhilation particularly through the exchange of the dark scalar doublet η and the charged singlet χ. Using MicrOMEGAs [121] to implement the Yukawa couplings of N_1 with ζ and χ indicates that the correct relic density can be reproduced with a choice of $f \approx 0.01$ and $f' \approx 0.5$. While f is required to produce the correct quark masses, the lepton masses are determined by two separate Yukawa couplings f' and the connection between the leptons and η [33]. Note this calculation has not taken into consideration the potential contributions to the relic density originating from the dark scalar doublet, which may reduce the size of f'; for the purposes of the collider searches the branching fraction of N_2 to e and μ being equal is more important than the absolute size of f'. Additionally, the LUX constraints on DM searches should be taken into account, however the spin-independent cross-section for $m_\zeta = 750$ GeV and $m_{N_1} = 160$ GeV produced in MicrOMEGAs is found to be well below the 2014 LUX limit [40].

For the analysis of potential signatures at the 13 TeV LHC, six cuts are applied to the signal and background events in PYTHIA, with four of the cuts corresponding to the cut regions from Ref. [116], while the last two cut regions are found to be effective for the scotogenic model [5]. All of the six cuts are described in Table 4.3 below, with the resulting $t\bar{t}$ decay cross section in each cut region. Each cut is implemented in PYTHIA 8 and applied to both the signal events, and the background events from $t\bar{t}$ decays. A signal-to-background (SB) ratio of the resulting cross sections is calculated for each choice of squark and DM mass. In Figs. 4.3 and 4.4 the regions in which the choice of DM mass and squark mass satisfies $SB > 5$ for various cuts are shown. Two of the cut regions, R1 and R4, do not have any mass choice for which $SB > 5$, and so do not appear in Figs. 4.3

and 4.4.

Cut:	E_T^{miss}	H_T	p_T^{j} (p_T^{l})	$\lvert\eta_{\text{j}}\rvert$ upper-limit	$\lvert\eta\rvert$ e (μ) upper-limit	σ_{cut} (fb)
R1	275	300	30 (20)	3.00	2.40 (2.50)	10.0
R2	200	600	30 (20)	3.00	2.40 (2.50)	0.5
R3	275	600	30 (20)	3.00	2.40 (2.50)	0.4
R4	200	$> 125, < 300$	30 (20)	3.00	2.40 (2.50)	33.1
R5	200	350	30 (20)	3.00	2.40 (2.50)	7.1
R6	200	350	150 (25)	3.00	2.40 (2.50)	1.2

Table 4.3: Cuts applied to the signal and background for opposite-sign opposite-flavor dileptons + 2 jets + missing energy (E_T^{miss}).

As seen in Figs. 4.3 and 4.4, the cuts R5 and R2 allow fewer mass choices to have a large SB ratio. This can be understood after consulting the resulting background cross sections in Table 4.3, which show that the background cross section for these cuts are larger than the cuts R6 and R3, so while fewer background events survive these more stringent cuts, the background events are cut down even further producing the results seen in Figs. 4.3 and 4.4. Based on the results from Ref. [5], the model discussed in this thesis has the

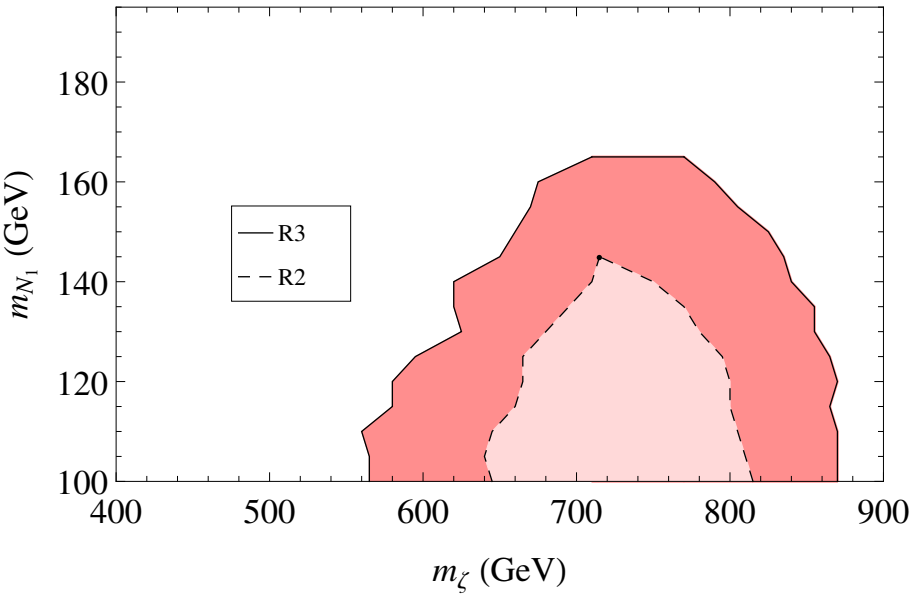

Figure 4.3: Masses for N_1 and ζ that yield a signal-to-background ratio larger than 5 under the R2 and R3 cuts described in Table 4.3

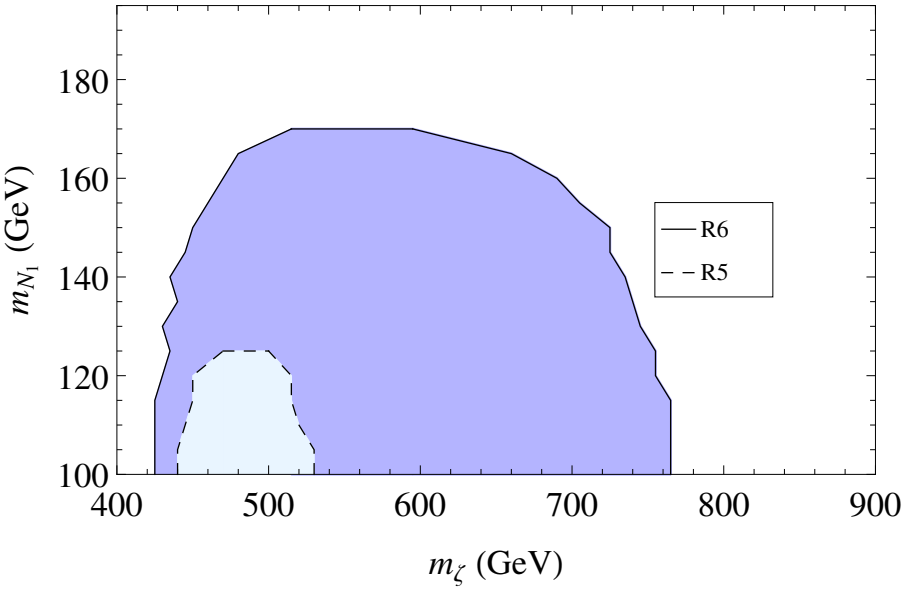

Figure 4.4: Masses for N_1 and ζ that yield a signal-to-background ratio larger than 5 under the R5 and R6 cuts described in Table 4.3

potential to be observed at the LHC during the 13 TeV run, and has a signature distinct from SUSY. The major difference between this model and SUSY is that the signature is produced solely in the opposite-flavor channel, however, same-sign searches use the opposite-flavor events to estimate the flavor symmetric background [113], and subtract it from the observed same-sign background to obtain a signal for SUSY [113]. Given a similar search strategy, our model would predict a significant negative signal in same-flavor searches. As a result, any large, positive, signal in the same-flavor channel could potentially rule out or heavily constrain our model. For example the mass choices that produce large SB ratios would be ruled out in such a scenario. In addition, searches at 13 TeV for ζ decaying directly to dN_1 will provide further constraints. With the full results of the 8 TeV run, a more detailed analysis to determine the full extent that SUSY searches constrain the scotogenic model is warranted.

Part III

Summary, Bibliography and Appendices

Chapter 5

Summary and Discussion

The discovery of θ_{13} being non-zero [47, 48] has opened the question: what, if any, flavor symmetry is the correct one to explain neutrino oscillation and flavor structure. Additionally, the discovery of a SM-like Higgs boson of 125 GeV [7, 8] has made the scotogenic mechanism first proposed in 2006 [32] to be of particular interest as it naturally accommodates flavor structure without the need for many additional scalars.

In Chapter 3, four models of neutrino oscillation have been analyzed, where the use of D_7 symmetry in a non-scotogenic model is easily contrasted with three examples of scotogenic models with various symmetries. The first scotogenic model considered connects the neutrino mass matrix to a neutral fermion mass matrix which had been studied previously in a non-scotogenic context, however the scotogenic model complicated the analysis of the neutrino mass mixing by the introduction of a logarithmic term which allowed different neutrino mass hierarchies and predictions that differed from the non-scotogenic neutrino mass texture. Before θ_{13} was known to be non-zero, two non-scotogenic models using the $\Delta(27)$ flavor symmetry had predicted $theta_{13} \neq 0$, and it was shown in Section 3.3 how both structures of neutrino mass matrix could be reproduced in either the minimal scotogenic model, or an extended scotogenic model where the dark symmetry is promoted to a $U(1)_D$ gauge symmetry (which could remain exact or be subsequently broken spontaneously). And lastly, a non-minimal scotogenic model with $\mu - \tau$ interchange symmetry was investigated

for the case when the ratio of the μ and τ Yukawa coupling constants was no-longer set to unity.

In Chapter 4, the collider signatures for a scotogenic model using an A_4 flavor symmetry and a mass scheme with a warm dark matter candidate was investigated, illustrating that the signature would be hard to distinguish from the SM background coming from W bosons. In the subsequent section a scotogenic mechanism that also incorporated quark and lepton mass, and utilizing a generic flavor symmetry to give a particular flavor structure of the Yukawa couplings, was investigated. The constraints from existing searches for SUSY were compared to such a model, and constraints from generic models of DM with a strongly coupled mediator were also considered. After considering these constraints, and simulating the scotogenic signal, it was found that for particular choice of masses a signal could potentially be found at the LHC run that is currently underway at a center of mass energy of 13 TeV. With the recent release of the full 8 TeV SUSY searches, it was also suggested that further analysis of the scotogenic model is warranted.

Bibliography

[1] E. Ma, A. Natale, and A. Rashed *Int. J. Mod. Phys.* **A27** (2012) 1250134, arXiv:1206.1570 [hep-ph].

[2] S. Bhattacharya, E. Ma, A. Natale, and D. Wegman *Phys. Rev.* **D87** (2013) 013006, arXiv:1210.6936 [hep-ph].

[3] S. Bhattacharya, E. Ma, A. Natale, and A. Rashed *Phys. Rev.* **D87** (2013) 013006, arXiv:1302.6266 [hep-ph].

[4] E. Ma and A. Natale *Phys. Lett.* **B723** (2014) 403–405, arXiv:1403.6772 [hep-ph].

[5] E. Ma and A. Natale *Phys. Lett.* **B740** (2015) 80–82, arXiv:1410.2902 [hep-ph].

[6] E. Ma, A. Natale, and O. Popov *Phys. Lett.* **B746** (2015) 114–116, arXiv:1502.08023 [hep-ph].

[7] A. Collaboration, G. Aad, *et al. Phys. Lett.* **B716** (2012) 1.

[8] C. Collaboration, S. Chatrchyan, *et al. Phys. Lett.* **B716** (2012) 30.

[9] M. Herrero hep-ph/9812242 [hep-ph].

[10] **Particle Data Group** Collaboration, K. Olive *et al. Chin. Phys.* **C38** (2014) 090001.

[11] **T2K** Collaboration, K. Abe *et al. Nucl. Instrum. Meth.* **A659** (2011) 106–136, arXiv:1106.1236 [hep-ex].

[12] **K2K** Collaboration, M. Ahn *et al. Phys. Rev.* **D74** (2006) 072003, hep-ex/0606032 [hep-ex].

[13] **KAMIOKANDE-II** Collaboration, K. Hirata *et al. Phys. Lett.* **B205** (1988) 416.

[14] **Super-Kamiokande** Collaboration, Y. Fukuda *et al. Phys. Rev. Lett.* **81** (1998) 1562–1567, hep-ex/9807003 [hep-ex].

[15] **Doulbe Chooz** Collaboration, Y. Abe *et al. Phys. Rev. Lett.* **108** (2012) 131801.

[16] **SNO** Collaboration, S. Ahmed *et al. Phys. Rev. Lett.* **92** (2004) 102004.

[17] **SNO** Collaboration, B. Aharmin *et al. Phys. Rev.* **C88** (2013) 025501.

[18] **KamLAND** Collaboration, K. Eguchi *et al. Phys. Rev. Lett.* **90** (2003) 021802, hep-ex/0212021 [hep-ex].

[19] **KamLAND** Collaboration, K. Eguchi *et al. Phys. Rev.* **D83** (2011) 052002, arXiv:1009.4771 [hep-ex].

[20] **ALEPH, DELPHI, L3, OPAL, and SLD** Collaboration, L. E. W. Group *Phys. Rept.* **427** (2006) 257.

[21] **Planck** Collaboration, P. Ade *et al.* arXiv:1502.01589 [astro-ph.CO].

[22] **WMAP** Collaboration, C. Bennet *et al. Astrophys. J.* **208** (2013) 20, arXiv:1212.5225 [astro-ph.CO].

[23] W. de Blok, S. McGaugh, A. Bosma, and V. Rubin *Astrophys. J.* **552** (2001) L23–L26, astro-ph/0103102 [astro-ph].

[24] P. Salucci and A. Borriello *Lect. Notes Phys.* **616** (2003) 66–77, astro-ph/0203457 [astro-ph].

[25] D. Reed, F. Governato, L. Verde, J. Gardern, T. Quinn, J. Stadel, D. Merritt, and G. Lake *Mon. Not. Roy. Astron. Soc.* **357** (2005) 82–96, astro-ph/0312544 [astro-ph].

[26] L. Koopmans and T. Treu *Astrophys. J.* **583** (2003) 606, astro-ph/0205281 [astro-ph].

[27] R. Metcalf, L. Moustakas, A. Bunker, and I. Parry *Astrophys. J.* **607** (2004) 43–59, astro-ph/0309738 [astro-ph].

[28] L. Moustakas and R. Metcalf *Mon.Not.Roy.Astron.Soc.* **339** (2003) 607.

[29] H. Hoekstra, H. Yee, and M. Gladders *New Astron. Rev.* **46** (2002) 767, astro-ph/0205205 [astro-ph].

[30] S. Vogt, M. Mateo, E. Olszewski, and M. Keane *Astron. Journal* **109** (1995) 151.

[31] M. Mateo *Ann. Rev. Astron. Astrophys.* **36** (1998) , astro-ph/9810070 [astro-ph].

[32] E. Ma *Phys. Rev.* **D73** (2006) 077301.

[33] S. Fraser and E. Ma *Europhys. Lett.* **108** (2014) 11002.

[34] E. Ma arXiv:1504.05503 [hep-ph].

[35] J. Bond and A. Szalay *Astrophys. J.* **274** (1983) 443.

[36] J. Bardeen, J. Bond, N. Kaiser, and A. Szalay *Astrophys. J.* **304** (1986) 15.

[37] G. Blumenthal, S. Faber, J. Primack, and M. Rees.

[38] J. Feng and J. Kumar *Phys. Rev. Lett.* **101** (2008) 231301, `arXiv:0803.4196 [hep-ph]`.

[39] M. Goodman and E. Witten *Phys. Rev.* **D31** (1985) 3059.

[40] **LUX** Collaboration, D. Akerib *et al. Phys. Rev. Lett.* **112** (2014) 091303.

[41] B. Moore *Nature* **370** (1994) 629.

[42] R. Flores and J. Primack *Astrophys. J.* **427** (1994) L1, `astro-ph/9402004 [astro-ph]`.

[43] M. Walker and J. Penarrubia *Astrophys. J.* **742** (2011) 20.

[44] R. Kuzio de Naray, S. McGaugh, and W. de Blok *Astrophys. J.* **676** (2008) 920.

[45] **DES** Collaboration, K. Bechtol *et al.* `arXiv:1503.02584 [astro-ph.GA]`.

[46] M. Kaplinghat, T. Linden, and H.-B. Yu *Phys. Rev. Lett.* **114** (2015) 211303, `arXiv:1501.03507 [hep-ph]`.

[47] **DAYA-BAY** Collaboration, F. An *et al. Phys. Rev. Lett.* **108** (2012) 171803, `arXiv:1203.1669 [hep-ex]`.

[48] **RENO** Collaboration, J. Ahn *et al. Phys. Rev. Let.*. **108** (2012) 191802, `arXiv:1204.0626 [hep-ex]`.

[49] E. Majorana *Il Nuovo Cimento* **14** (1937) 171–184.

[50] S. Weinberg *Phys. Rev. Lett.* **43** (1979) 1566.

[51] M. Gell-Mann, P. Rmmond, and R. Slansky, *Supergravity*. North-Holland, Amsterdam, 1979.

[52] T. Yanagida, *Proceedings of the Workshop on the Unified Theory and the Baryon Number in the Universe*. Tsukuba, Japan, 1979.

[53] R. N. Nohapatra and G. Senjanovic *Phys. Rev. Lett.* **44** (1980) 912.

[54] J. Schechter and J. Valle *Phys. Rev.* **D22** (1980) 2227.

[55] E. Ma and U. Sarkar *Phys. Rev. Lett.* **80** (1998) 5716.

[56] R. Foot, H. Lew, X.-G. He, and G. Joshi *Z. Phys.* **C44** (1989) 441.

[57] F. Bonnet, M. Hirsch, T. Ota, and W. Winter *JHEP* **07** (2012) 153, `arXiv:1204.5862 [hep-ph]`.

[58] A. Zee *Phys. Lett.* **B93** (1980) 389.

[59] R. Mohapatra *Phys. Rev. Lett.* **56** (1986) 561.

[60] R. N. Mohapatra and J. Valle *Phys. Rev.* **D34** (1986) 1642.

[61] Z. Maki, M. Nakagawa, and S. Sakata *PTP* **28** (1962) 870.

[62] B. Pontecorvo *JETP* **6** (1957) 429.

[63] P. Harrison, D. Perkins, and W. Scott *Phys. Lett.* **B458** (1999) 79.

[64] E. Ma and G. Rajasekaran *Phys. Rev.* **D64** (2001) 113012.

[65] E. Ma *Phys. Lett.* **A17** (2002) 2361.

[66] K. Babu, E. Ma, and J. Valle *Phys. Lett.* **B552** (2003) 207–213, hep-ph/0206292 [hep-ph].

[67] E. Ma *Mod. Phys. Lett* **A21** (2006) 1917, hep-ph/0607190 [hep-ph].

[68] E. Ma *Phys. Lett.* **B660** (2008) 505, arXiv:0709.0507 [hep-ph].

[69] H. Ishimori and E. Ma *Phys. Rev.* **D86** (2012) 045030, arXiv:1205.0075 [hep-ph].

[70] E. Ma arXiv:1502.02200 [hep-ph].

[71] E. Ma *Phys. Rev.* **D73** (2006) 057304, arXiv:hep-ph/0511133 [hep-ph].

[72] S. Fraser, E. Ma, and O. Popov *Phys. Lett.* **B737** (2014) 280, arXiv:1408.4785 [hep-ph].

[73] E. Ma *Phys. Rev. Lett.* **112** (2013) 091801, arXiv:1311.3213 [hep-ph].

[74] H. Georgi and S. Glashow *Phys. Rev. Lett.* **32** (1974) 438–441.

[75] R. Mohapatra and M. Parida *Phys. Rev.* **D47** (1993) 264.

[76] D. Lee *et al. Phys. Rev.* **D51** (1995) 229.

[77] I. Dorsner and P. Perez *Phys. Lett.* **B642** (2006) 248–252, arXiv:hep-ph/0606062 [hep-ph].

[78] K. Schnitter *JHEP* **1305** (2013) 151, arXiv:1204.2111 [hep-ph].

[79] S.-L. Chen and E. Ma *Phys. Lett.* **B620** (2005) .

[80] Z. Z. Xing, H. Zhang, and S. Zhou *Phys. Rev.* **D77** (2008) 113016.

[81] **Particle Data Group** Collaboration, J. Beringer *et al. Phys. Rev.* **D80** (2012) 010001.

[82] C. Jarlskog *Z. Phys.* **C29** (1985) 491.

[83] E. Ma *Phys. Rev.* **D70** (2004) 031901, hep-ph/0404199 [hep-ph].

[84] H. Ishimori, T. Kobayashi, H. Ohki, H. Okada, Y. Shimizu, and M. Tanimoto *Prog. Theor. Phys. Suppl.* **183** (2010) 1–163, arXiv:1003.3552 [hep-ph].

[85] G. Branco, J. Gerard, and W. Grumus *Phys. Lett.* **B136** (1984) 383.

[86] E. Ma, I. Picek, and B. Radovcic *Phys. Lett.* **B726** (2013) 744, arXiv:1308.5313 [hep-ph].

[87] W. Grimus and L. Lavoura *Phys. Lett.* **B579** (2004) 113.

[88] E. Ma *Phys. Rev.* **D66** (2002) 117301, hep-ph/0207352 [hep-ph].

[89] E. Ma *Phys. Rev. Lett.* **81** (1998) 1171.

[90] J. Alwall, R. Frederix, S. Frixione, V. Hirschi, F. Maltoni, O. Mattelaer, H.-S. Shao, T. Stelzer, P. Torrielli, and M. Zaro *JHEP* **1407** (2014) 079, arXiv:1405.0301 [hep-ph].

[91] A. P. A. Belyaev, C.D. Neil *Comput. Phys. Commun.* **189** (2013) 1729, arXiv:1207.6082 [hep-ph].

[92] T. Sjöstrand, S. Mreena, and P. Skands *JHEP* **0605** (2006) 026.

[93] T. Sjöstrand, S. Mreena, and P. Skands *Comput. Phys. Comm.* **178** (2008) 852.

[94] M. Cacciari, G. Salam, and G. Soyez *EPJ* **C71** (2012) 1896, arXiv:1111.6097 [hep-ph].

[95] H. de Vega and N. Sanchez arXiv:1109.3187 [astro-ph.CO].

[96] H. de Vega and N. G. Sanchez arXiv:1203.3562 [astro-ph.CO].

[97] C. Watson, Z. Li, and N. K. Polley *JCAP* **1203** (2012) 018.

[98] M. Viel, G. D. Becker, J. S. Bolton, M. G. Haehnelt, M. Rauch, and W. L. W. Sargent *Phys. Rev. Lett.* **100** (2008) 041304.

[99] K. Abazajian *et al.* arXiv:1204.5379 [hep-ph].

[100] E. Ma and M. Raidal *Phys. Rev. Lett.* **87** (2001) 011802, hep-ph/0102255 [hep-ph].

[101] A. Pierce and J. Thaler *JHEP* **0708** (2007) 026, hep-ph/0703056 [hep-ph].

[102] P. Posch *Phys. Lett.* **B696** (2011) 447.

[103] A. Arhrib, R. Benbrik, and N. Gaur *Phys. Rev.* **D85** (2012) 095021.

[104] J. Chang, K. Cheung, P.-Y. Tseng, and T.-C. Yuan *Int. J. Mod. Phys.* **A27** (2012) 1230030.

[105] B. Swiezewska and M. Krawczyk *Phys. Rev.* **D88** (2012) 035019, arXiv:1212.4100 [hep-ph].

[106] C. Collaboration *Phys. Lett.* **B710** (2012) 403, arXiv:1202.1487 [hep-ex].

[107] A. Collaboration arXiv:1504.05833 [hep-ex].

[108] **CTEQ** Collaboration, H. Lai *et al. Eur. Phys. J.* **C12** (2000) 375.

[109] E. Ma *Phys. Lett.* **B659** (2008) 885–887, arXiv:0710.2325 [hep-ph].

[110] J. Pumplin *et al. JHEP* **0207** (2002) 012.

[111] A. Alloul, N. D. Christensen, C. Degrande, C. Duhr, and B. Fuks *Comput. Phys. Comm.* **185** (2014) 2250.

[112] C. Borschensky, M. Kramer, A. Kulesza, M. Mangano, S. Padhi, T. Plehn, and X. Portell arXiv:1407.5066 [hep-ph].

[113] CMS Collaboration Tech. Rep. CMS-PAS-SUS-12-019, 2012. http://cdsweb.cern.ch/record/1751493.

[114] M. Czakon, P. Fiedler, and A. Mitov *Phys. Rev. Lett.* **110** (2013) 252004, arXiv:1303.6254 [hep-ph].

[115] CMS Collaboration Tech. Rep. CMS-PAS-SUS-13-019, 2013. http://cds.cern.ch/record/1646394.

[116] CMS Collboration *Phys. Rev.* **D88** (2013) 052017, arXiv:1206.3949 [hep-ex].

[117] S. Chang, R. Edezhath, J. Hutchinson, and M. Luty *Phys. Rev.* **D89** (2014) 015011, arXiv:1307.8120 [hep-ph].

[118] H. An, L.-T. Wang, and H. Zhang *Phys. Rev.* **D89** (2014) 115014, arXiv:1308.0592 [hep-ph].

[119] A. DiFranzo, K. I. Nagao, A. Rajaraman, and T. M. P. Tait *JHEP* **1311** (2013) 014, arXiv:1308.2679 [hep-ph].

[120] Y. Bai and J. Berger *JHEP* **1311** (2013) 171, arXiv:1308.0612 [hep-ph].

[121] G. Belanger, F. Boudjema, A. Pukhov, and A. Semenov, 2015.

[122] M. E. Peskin and D. V. Schroeder, *An Introduction to Quantum Field Theory.* Perseus Books, 1st ed., 1995.

[123] E. Ma *Phys. Lett.* **B717** (2012) 235.

[124] H. Jones, *Groups, Representations and Physics.* CRC Press, 2nd ed., 1998.

[125] H. Weber and G. Arfken, *Essential Mathematical Methods for Physicists*. Elsevier Acadmeic Press, 525 B Stree, Suite 1900, San Diego, CA 92101-4495, USA, 1st ed., 2004.

[126] W. Grimus and P. Ludl *J. Phys.* **A43** (2010) 445209, arXiv:1006.0098 [hep-th].

[127] C. Luhn, S. Nasri, and P. Ramond *J. Math. Phys.* **48** (2007) 073501, hep-th/0701188 [hep-th].

Appendix A

Scotogenic Loop Calculation

The loop generation of neutrino mass is guaranteed to be finite, but counting the superficial degree of divergence of the diagrams leads one to believe that these should diverge. However, as stated in the body of the thesis, there is a mass splitting between the scalar degrees of freedom and thus the loop cancels. In order to calculate the loop from the scotogenic diagram in Fig. A.1, it is necessary to first re-draw the diagram. The literature usually displays the diagram in a way so that the nature of the five dimensional operator is manifest, but when calculating the loop it is crucial to only use the mass eigenstates of the problem. As such the diagram that the loop comes from can be re-drawn as seen in

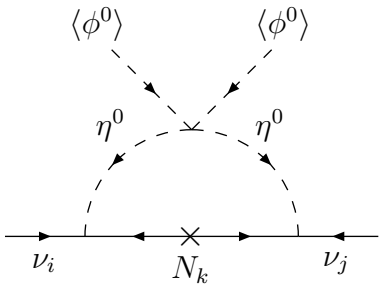

Figure A.1: The minimal scotogenic mechanism.

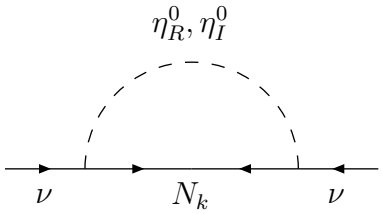

Figure A.2: Scotogenic loop diagram using mass eigenstates

Fig. A.2, and this diagram results in the integral of the form:

$$I = \sum_k \int \frac{d^4k}{(2\pi)^4}(\not{k} + m_{N_k}) \left[\frac{i}{(k^2 - m_{N_k}^2)(k^2 - m_R^2)} - \frac{i}{(k^2 - m_{N_k}^2)(k^2 - m_I^2)} \right] \tag{A.1}$$

$$= \sum_k \int \frac{d^4k}{(2\pi)^4} i(\not{k} + m_{N_k}) \left[\frac{m_R^2 - m_I^2}{(k^2 - m_{N_k}^2)(k^2 - m_R^2)(k^2 - m_I^2)} \right]$$

To perform this integral, the propagators will be combined following the Feynman parameter prescription (see Ref. [122]). For n propagators (labeled A_n), each copied m_i times in the denominator, we can use the following general formula [122]:

$$\frac{1}{A_1^{m_1} A_2^{m_2} \dots A_n^{m_n}} = \int_0^1 dx_1 \dots dx_n \delta\left(\sum x_i - 1\right) \frac{\Pi x_i^{m_i - 1}}{(\sum x_i A_i)^{\sum m_i}} \frac{\Gamma(\sum m_i)}{\Gamma(m1) \dots \Gamma(m_n)} \tag{A.2}$$

The above integral can thus be re-written (after taking into account the Dirac delta function):

$$I = \sum_k i(m_R^2 - m_I^2) \int \frac{d^4k}{(2\pi)^4}(\not{k} + m_{N_k}) \int_0^1 dx \int_0^{1-x} dy \Gamma(3)$$
$$\times (x(k^2 - m_{N_k}^2) + y(k^2 - m_R^2) + (1 - x - y)(k^2 - m_I^2))^{-3}$$

Rearranging the denominator:

$$I = 2\sum_k i(m_R^2 - m_I^2)\int_0^1 dx\int_0^{1-x} dy\int \frac{d^4k}{(2\pi)^4}\frac{\not{k} + m_{N_k}}{(k^2-\Delta)^3},$$
$$\text{where } \Delta = x(m_{N_k}^2 - m_I^2) + y(m_R^2 - m_I^2) + m_I^2$$

The integral over $\not{k}$ goes to zero by symmetry. Using a Wick rotation ($k_0 = il_0$ so that $k^2 \to -l^2$) the integral over k can be performed in a four-dimensional spherical space:

$$\begin{aligned}
I &= 2\sum_k \frac{m_{N_k}(m_R^2 - m_I^2)}{(2\pi)^4}\int_0^1 dx\int_0^{1-x} dy\int l^3 dl d\Omega \frac{1}{\Delta^3(1+l^2/\Delta)^3} \\
&= 2\sum_k \frac{m_{N_k}(m_R^2 - m_I^2)}{(2\pi)^4}\int_0^1 dx\int_0^{1-x} dy\int 2\pi^2 \frac{l^3 dl}{\Delta^3(1+l^2/\Delta)^3} \\
&= \sum_k \frac{m_{N_k}(m_R^2 - m_I^2)}{4\pi^2}\int_0^1 dx\int_0^{1-x} dy\int_0^{\frac{\pi}{2}} \Delta^{-1}\cos\theta\sin^3\theta d\theta \\
&= \sum_k \frac{m_{N_k}(m_R^2 - m_I^2)}{16\pi^2}\int_0^1 dx\int_0^{1-x} dy \frac{1}{x(m_{N_k}^2 - m_I^2) + y(m_R^2 - m_I^2) + m_I^2} \\
&= \sum_k \frac{m_{N_k}(m_R^2 - m_I^2)}{16\pi^2}\int_0^1 dx \log\left[\frac{x(m_{N_l}^2 - m_R^2) + m_R^2}{x(m_{N_k}^2 - m_I^2) + m_I^2}\right]
\end{aligned}$$

The final integral can be performed by taking the derivative under the integral sign, and the final result — with Yukawa couplings h_{ij} — is:

$$I = \sum_k \frac{h_{ik}h_{jk}m_{N_k}}{16\pi^2}\left[\frac{m_R^2}{m_R^2 - m_{N_k}^2}\log(m_R^2/m_{N_k}^2) - \frac{m_I^2}{m_I^2 - m_{N_k}^2}\log(m_I^2/m_{N_k}^2)\right] \tag{A.3}$$

The above is the full solution to the basic scotogenic model, but there are several key approximations that have also been considered in the literature. As stated, the mass splitting from the real and imaginary components of η are related to λ_5 ($m_R^2 - m_I^2 = 2\lambda_5 v^2$). If this splitting is small compared to $m_0 = (m_R^2 + m_I^2)/2$ then Eq. A.3 can be re-written:

$$\mathcal{M}_{ij} \approx \sum_k h_{ij}h_{jk}\frac{m_{N_k}}{16\pi^2}\left[\frac{m_0^2+\lambda_5 v^2}{(m_0^2-m_{N_k}^2)}\log(m_I^2) - \log(m_R^2)\frac{m_0^2-\lambda_5 v^2}{(m_0^2-m_{N_k}^2)}\right]$$
$$- \sum_k h_{ij}h_{jk}\frac{m_{N_k}}{16\pi^2}\left[\frac{2_5 v^2}{m_0^2-m_{N_k}^2}\log(m_{N_k}^2)\right]$$
$$= \sum_k h_{ij}h_{jk}\frac{m_{N_k}}{16\pi^2(m_0^2-m_{N_k}^2)}\left[2\lambda_5 v^2(-log(m_{N_k}^2)+log(m_0^2)) + m_0^2(log(m_I^2/m_R^2))\right]$$

The $\log(m_I^2/m_R^2)$ term is written in terms of this mass splitting yielding $\log\left[\frac{1+\lambda_5 v^2}{1-\lambda_5 v^2}\right]$ and expanded ($\lambda_5 v^2 \ll m_0^2$). Substituting this expression into $\mathcal{M}_{ij}$ yields:

$$\mathcal{M}_{ij} = \sum_k h_{ij}h_{jk}\frac{\lambda_5 v^2 m_{N_k}}{8\pi^2(m_0^2-m_{N_k}^2)}\left[1 - \frac{M_{N_k}^2}{m_0^2-m_{N_k}^2}\log\left(\frac{m_0^2}{m_{N_k}^2}\right)\right] \tag{A.4}$$

This form of the scotogenic mass was first considered in Ref. [32]. Additionally, if $m_0^2 \ll M_k^2$ then Eq. A.3 can be simplified:

$$\mathcal{M}_{ij} \approx \sum_k h_{ij}h_{jk}\frac{m_{N_k}}{16\pi^2}\left[\frac{m_0^2+\lambda_5 v^2}{(-m_{N_k}^2)(1-m_R^2/m_{N_k}^2)}(\log(m_R^2)\right]$$
$$- \sum_k h_{ij}h_{jk}\frac{m_{N_k}}{16\pi^2}\left[\log(m_{N_k}^2)) - (\log(m_I^2)-\log(m_{N_k}^2))\frac{m_0^2-\lambda_5 v^2}{(-m_{N_k}^2)(1-m_I^2/m_{N_k}^2)}\right]$$
$$= \sum_k h_{ij}h_{jk}\frac{m_{N_k}}{16\pi^2}\left[2\lambda_5 v^2(log(m_{N_k}^2)-log(m_0^2)) - m_0^2(log(m_I^2/m_R^2))\right]$$

Just as for Eq. A.4, the $\log(m_I^2/m_R^2)$ yields

$$\mathcal{M}_{ij} = \sum_k h_{ij}h_{jk}\frac{\lambda_5 v^2}{8\pi^2 m_{N_k}}\left[\log\left(\frac{m_{N_k}^2}{m_0^2}\right) - 1\right]. \tag{A.5}$$

This results in a seesaw like neutrino mass, modified by a log term, and is thus called the radiative seesaw where deviations from a typical seesaw mechanism come in the form of the logarithmic corrections. An analysis of a particular implementation of this mass-scheme is discussed in Ref. [1]. If the splitting is taken to be small, but $m_0^2 \gg m_{N_k}^2$, Eq. A.3 is approximated by a straightforward seesaw equation:

$$\mathcal{M}_{ij} = \sum_k h_{ij} h_{jk} \frac{\lambda_5 v^2}{8\pi^2} \frac{m_{N_k}}{m_0^2} \tag{A.6}$$

As pointed out in Ref. [123], if we do not make assumptions about the splitting between m_R^2 and m_I^2, but rather assume $m_{N_k}^2 \ll m_R^2, m_I^2$, then Eq. A.3 is approximately

$$\mathcal{M}_{ij} = \sum_k h_{ij} h_{jk} \frac{\log(m_R^2/m_I^2) m_{N_k}}{16\pi^2}, \tag{A.7}$$

which results in an inverse seesaw mechanism in order to generate small neutrino mass, and is implemented and analyzed in Ref. [3].

Appendix B

Inverse Scotogenic Loop Calculation

To illustrate how the mass is calculated for the scotogenic mechanism depicted in Fig. B.1 and analyzed in Ref. [6], the amplitude will be written out explicitly in terms of fields, and then contracted in order to carefully take into account the chirality of particles within the loop and properly deal with the Majorana mass terms that complete the loop. The Yukawa term generating the mass is $fs\bar{E}^0_R\nu_L$, which can be re-written using the chirality projection operators defined as:

$$P_R = \frac{1+\gamma_5}{2} \tag{B.1}$$

$$P_L = \frac{1-\gamma_5}{2}. \tag{B.2}$$

To generate the mass term $\bar{\nu}^c\nu$, the amplitude is given by the contribution from the m_R mass insertion

$$\langle \text{out} \mid (\bar{\nu}^c P_L E^c_R s)(m_R \bar{N}^c_R N_R)(s\bar{E}_R P_L \nu) \mid \text{in}\rangle, \tag{B.3}$$

and the contribution from the m_L mass insertion

$$\langle \text{out} \mid (\bar{\nu}^c P_L E_R^c s)(m_L \bar{N}_L^c N_L)(s \bar{E}_R P_L \nu) \mid \text{in} \rangle, \tag{B.4}$$

where the external momentum is set to zero, the Yukawa coupling constant f^2 has been set to 1 and the integral over the loop momentum k has been omitted for notational simplicity. Note that there is no factor of $1/2$ in the mass insertions; this is to properly take into account either the two possible Majorana contractions due to the Majorana mass or a definition of the Feynman rules for the mass insertion that properly takes this into account. The mass

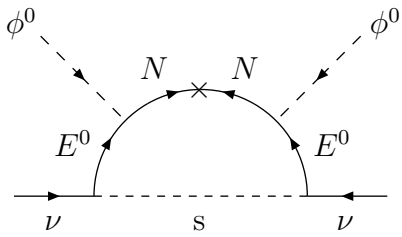

Figure B.1: The scotogenic mechanism for inverse seesaw neutrino mass.

eigenstates are actually given by $\omega_{1,2}$ which are related to $E_{R,L}$ and $N_{R,L}$ via

$$\begin{pmatrix} N_{(R,L)} \\ E_{(R,L)} \end{pmatrix} = \begin{pmatrix} \cos\theta_{(R,L)} & \sin\theta_{(R,L)} \\ -\sin\theta_{(R,L)} & \cos\theta_{(R,L)} \end{pmatrix} \begin{pmatrix} \omega^1_{(R,L)} \\ \omega^2_{(R,L)} \end{pmatrix}. \tag{B.5}$$

Using the notation that $\cos\theta_{R,L} = c_{R,L}$ and $\sin\theta_{R,L} = s_{R,L}$ then the amplitude becomes

$$\langle \text{out} \mid [\bar{\nu}^c P_L (c_R \omega_2^c - s_R \omega_1^c) s]\, [m_R (c_R \bar{\omega}_1^c + s_R \bar{\omega}_2^c) P_R (c_R \omega_1 + s_R \omega_2)]\, [s(c_R \bar{\omega}_2 - s_R \bar{\omega}_1) P_L \nu] \mid \text{in} \rangle,$$

for m_R and

$$\langle \text{out} \mid [\bar{\nu}^c P_L (c_R \omega_2^c - s_R \omega_1^c) s]\, [m_R (c_L \bar{\omega}_1^c + s_L \bar{\omega}_2^c) P_L (c_L \omega_1 + s_L \omega_2)]\, [s(c_R \bar{\omega}_2 - s_R \bar{\omega}_1) P_L \nu] \mid \text{in} \rangle,$$

for m_L. As described in many Quantum Field Theory books, and in particular Ref. [122], we now perform the contracts of the fields $\omega_{1,2}$ where the non-zero contractions are of the following form for the m_R component

$$\langle \text{out} \mid [\bar{\nu}^c P_L(c_R\omega_2^c - s_R\omega_1^c)s]\,[m_R(c_R\bar{\omega}_1^c + s_R\bar{\omega}_2^c)P_R(c_R\omega_1 + s_R\omega_2)]\,[s(c_R\bar{\omega}_2 - s_R\bar{\omega}_1)P_L\nu] \mid \text{in}\rangle,$$

and for the m_L component of the form

$$\langle \text{out} \mid [\bar{\nu}^c P_L(c_R\omega_2^c - s_R\omega_1^c)s]\,[m_L(c_L\bar{\omega}_1^c + s_L\bar{\omega}_2^c)P_L(c_L\omega_1 + s_L\omega_2)]\,[s(c_R\bar{\omega}_2 - s_R\bar{\omega}_1)P_L\nu] \mid \text{in}\rangle.$$

These contractions yield the usual fermion propagator in momentum space

$$D_i = \omega_i\bar{\omega}_i = \omega_i^c\bar{\omega}_i^c = \frac{i(\not{k} + m_i)}{k^2 - m_i^2}, \tag{B.6}$$

while the contraction of s yields the usual scalar propagator

$$D_s = \frac{i}{k^2 - m_s^2}. \tag{B.7}$$

For the m_R the propagators are thus

$$c_R^2 s_R^2 P_L(D_1 P_R D_1 - D_1 P_R D_2 - D_2 P_R D_1 + D_2 P_R D_2)P_L, \tag{B.8}$$

which can be simplified via

$$P_L D_i P_R D_j P_L = P_L \frac{\not{k} + m_i}{k^2 - m_i^2} P_R \frac{\not{k} + m_j}{k^2 - m_j^2} P_L \tag{B.9}$$

$$= P_L \frac{\not{k}}{k^2 - m_i^2} \frac{\not{k}}{k^2 - m_j^2} P_L \tag{B.10}$$

$$= P_L \frac{k^2}{(k^2 - m_i^2)(k^2 - m_j^2)} P_L, \tag{B.11}$$

Applying the P_L operators to either ν or $\bar{\nu}^c$, and using Eq. B.11, allows Eq. B.8 to be further simplified

$$= c_R^2 s_R^2 k^2 \left(\frac{1}{(k^2 - m_1^2)^2} + \frac{1}{(k^2 - m_1^2)^2} - \frac{2}{(k^2 - m_1^2)(k^2 - m_2^2)} \right) \tag{B.12}$$

$$= c_R^2 s_R^2 \frac{k^2}{(k^2 - m_1^2)^2 (k^2 - m_2^2)^2} \left((k^2 - m_1^2)^2 + (k^2 - m_2^2)^2 - 2(k^2 - m_1^2)(k^2 - m_2^2) \right) \tag{B.13}$$

$$= c_R^2 s_R^2 \frac{k^2}{(k^2 - m_1^2)^2 (k^2 - m_2^2)^2} \left(m_1^4 + m_2^4 - 2(m_1^2 m_2^2) \right). \tag{B.14}$$

Taking into account the Yukawa couplings, the common factor of D_s, and the integral over the loop momentum k yields the final contribution to m_ν from the insertion of m_R:

$$m_\nu^R = f^2 m_R \cos^2\theta_R \sin^2\theta_R (m_1^2 - m_2^2)^2 \int \frac{d^4k}{(2\pi)^4} \frac{k^2}{(k^2 - m_s^2)(k^2 - m_1^2)^2 (k^2 - m_2^2)^2}. \tag{B.15}$$

For the m_L contribution:

$$P_L (s_R^2 c_L^2 D_1 P_L D_1 - c_R s_R c_L s_L D_1 P_L D_2 - c_R s_R c_L s_L D_2 P_L D_1 + c_R^2 s_L^2 D_2 P_L D_2) P_L, \tag{B.16}$$

where

$$P_L D_i P_L D_j P_L = P_L \frac{\not{k} + m_i}{k^2 - m_i^2} P_L \frac{\not{k} + m_j}{k^2 - m_j^2} P_L \tag{B.17}$$

$$= P_L \frac{m_i m_j}{(k^2 - m_i^2)(k^2 - m_j^2)}. \tag{B.18}$$

After taking into account Yukawa couplings, and the common factor of D_s and the integral over the loop momentum k yields the final contribution to m_{nu} from m_L:

$$\begin{aligned} m_\nu^L &= f^2 m_L \sin^2\theta_R \cos^2\theta_L m_1^2 \int \frac{d^4k}{(2\pi)^4} \frac{1}{(k^2-m_s^2)(k^2-m_1^2)^2} \\ &+ f^2 m_L \cos^2\theta_R \sin^2\theta_L \int \frac{d^4k}{(2\pi)^4} \frac{1}{(k^2-m_s^2)(k^2-m_2^2)^2} \\ &- 2f^2 m_L \cos\theta_R \sin\theta_R \cos\theta_L \sin\theta_L \int \frac{d^4k}{(2\pi)^4} \frac{1}{(k^2-m_s^2)(k^2-m_1^2)(k^2-m_2^2)} \end{aligned} \tag{B.19}$$

As a result the total m_ν is given by Eq. 3.87 from Ref. [6]:

$$\begin{aligned} m_\nu &= f^2 m_R \cos^2\theta_R \sin^2\theta_R (m_1^2-m_2^2)^2 \int \frac{d^4k}{(2\pi)^4} \frac{k^2}{k^2-m_s^2} \frac{1}{(k^2-m1^2)^2} \frac{1}{(k^2-m2^2)^2} \\ &+ f^2 m_L m_1^2 \cos^2\theta_R \sin^2\theta_L \int \frac{d^4k}{(2\pi)^4} \frac{1}{k^2-m_s^2} \frac{1}{(k^2-m1^1)^2} \\ &+ f^2 m_L m_2^2 \sin^2\theta_R \cos^2\theta_L \int \frac{d^4k}{(2\pi)^4} \frac{1}{k^2-m_s^2} \frac{1}{(k^2-m2^2)^2} \\ &- 2f^2 m_L m_1 m_2 \cos\theta_R \sin\theta_R \cos\theta_L \sin\theta_L \int \frac{d^4k}{(2\pi)^4} \frac{1}{k^2-m_s^2} \frac{1}{k^2-m1^2} \frac{1}{k^2-m2^2} \end{aligned} \tag{B.20}$$

Appendix C

Group Theory

C.1 Review of Group Theory

In this Appendix, I summarize the basic facts of group theory without proof, for useful proofs see [84, 124–127]. A set, $\mathcal{G}$, is a group if it satisfies the following properties:

1. **Closure:** Given any two elements of $\mathcal{G}$ such that $a, b \in \mathcal{G}$, then $ab = c \in \mathcal{G}$ [84,124,125]
2. **Associativity:** Given $a, b, c \in \mathcal{G}$ then $(ab)c = a(bc)$ [84, 124, 125]
3. **Identity:** The set $\mathcal{G}$ includes an element, e, such that for any $a \in \mathcal{G}$ then ae = ea = a. [84, 124, 125]
4. **Inverse:** For any $a \in \mathcal{G}$ there exists an element, a^{-1}, such that $aa^{-1} = a^{-1}a = e$. [84, 124, 125]

Any set that satisfies all of the above criteria is hereto referred to, simply, as a group. It is useful to quickly list some of the basic properties of groups:

- **Order:** the order of a group, $\mathcal{G}$, is defined as the number of elements in $\mathcal{G}$. Elements in $\mathcal{G}$ can also have an order if there exists some number, x, such that $a^x = e$ [84, 124]

- **Abelian:** A group, $\mathcal{G}$, is called Abelian if any element $a, b \in \mathcal{G}$ satisfies $ab = ba$ (ie $\mathcal{G}$ is Abelian if every element commutes with every other element). If a group does not satisfy this, it is called **non-Abelian** [84, 124].

- **Subgroup:** A group, $\mathcal{H}$, is a subgroup of group $\mathcal{G}$ if every element in $\mathcal{H}$ is also in $\mathcal{G}$ and if the order of $\mathcal{H}$ is a factor of the order of $\mathcal{G}$ [84, 124].

- **Conjugate:** Elements in a group, $a, b \in \mathcal{G}$, are called conjugate elements if there exists some element, $c \in \mathcal{G}$, such that $c^{-1}ac = b$ [84, 124].

- **Conjugacy Class:** Conjugacy class is the set of all elements conjugate to an element, $a \in \mathcal{G}$. That is, the set of all c such that $c^{-1}ac, \forall c \in \mathcal{G}$ [84, 124].

There are many additional properties beyond these rudimentary features, and group theory is a wide and rich topic of mathematical inquiry. One of the more interesting aspects of groups is known as the representation of a group. A **representation** of a group is a one-to-one mapping of elements of the group $\mathcal{G}$ onto matrices and is denoted as $D(g)$ for $g \in \mathcal{G}$, and any representation $D(g)$ also satisfies the properties of a group (i.e. closure, associativity, identity, inverse, and whether or not the matrix representations of group elements commute or not) [84, 124, 126, 127]. The vector space that these matrices, $D(g)$, act on is known as the **representation space**, and the dimension of the representation space is equal to the dimension of the representation. If we take a vector from the representation space of $D(g)$, and if $D(g)$ acting on a vector from the subspace produces another vector in that same subspace, then the representation is referred to as **reducible** [84]. An **irreducible** representation is thus a representation where there is no such invariant subspace. In short, these properties allow us to write any reducible representation of the group $\mathcal{G}$ as a direct sum of irreducible representations. This has a familiar application in the form Young tableau [124], which allows us to write products of non-Abelian continuous groups as sums of irreducible representations. A similar decomposition also exists for products of discrete group representations, but the finite number of elements reduces these rules to a

handful. Additionally, the **character** of a representation can be defined as the trace of the representation of an element of the group [84, 124, 126, 127]

$$\chi_i(g) = \mathrm{tr}(D_i(g)), \tag{C.1}$$

which also obey an orthogonality relation

$$\sum \chi_\alpha(g_i)\chi^*_\beta(g_j) = \delta_{ij}\delta_{\alpha\beta}\frac{N_\mathcal{G}}{n_i}, \tag{C.2}$$

where α and β represent different representations of the form $D_\alpha(g_i)$, $N_\mathcal{G}$ is the order of the group G, and n_i are the number of elements in the conjugacy class C_i for element g_i. The orthogonality relation in Eq. C.2 necessarily implies that elements in the same conjugacy class will have the same character for a particular dimension of representation [84], and also leads to the following relation [84, 124]:

$$\sum_\alpha \chi^2_\alpha(C) = \sum_n m_n n^2 = N_\mathcal{G}, \tag{C.3}$$

where n is the dimensionality of the representation, and m_n is the dimensionality of the representation that must satisfy $\sum_n m_n = N_C$, where N_C is the number of conjugacy classes. Thus, using these relations and knowing the order of the group it is possible to determine the dimensionality of representations of the discrete group. An interesting result, quoted without proof, is that the number of irreducible representations is equal to the number of conjugacy classes [84].

C.2 Non-Abelian Discrete Groups

All of the non-Abelian discrete groups discussed in this thesis are finite subgroups of $SU(3)$, and many of these can be organized into the "dihedral-like" [126] subgroups labeled either as $\Delta(3n^2)$ or $\Delta(6n^2)$ where $\Delta(12)$ is isomorphic to A_4 (for n= 2 and $\Delta(3n^2)$)

and $\Delta(6)$ is isomiorphic to S_4 (for n =1 and $\Delta(6n^2)$) [84,126]. For a general n in $\Delta(3n^2)$ and $\Delta(6n^2)$ the conjugacy classes, character tables, and multiplication rules have been worked out in full detail in, for instance, Refs. [84, 127]. For the purposes of this brief review, the smallest non-Abelian discrete group, S_3, will be worked out in some detail followed by a general discussion of the discrete groups relevant to the work in this thesis.

C.3 S_3

The non-Abelian discrete group S_3 is the set of all permutations among three objects, with each element representing a distinct permutation of three objects as illustrated below [84, 124]:

$$e_1 : (a_1, a_2, a_3) \to (a_1, a_2, a_3)$$
$$e_2 : (a_1, a_2, a_3) \to (a_2, a_1, a_3)$$
$$e_3 : (a_1, a_2, a_3) \to (a_3, a_2, a_1)$$
$$e_4 : (a_1, a_2, a_3) \to (a_1, a_3, a_2)$$
$$e_5 : (a_1, a_2, a_3) \to (a_3, a_1, a_2)$$
$$e_6 : (a_1, a_2, a_3) \to (a_2, a_3, a_1)$$

Note that the element e_1 can be considered the identity element for this group. The multiplication of the above 6 elements are closed under multiplication in that the maps occur additively, so that $e_3 e_4$ yields the permutation

$$e_3 e_4 : (a_1, a_2, a_3) \to_{e_3} (a_3, a_2, a_1) \to_{e_4} (a_3, a_1, a_2) = e_5. \tag{C.4}$$

Because of this property of closure, these elements can be re-written as the set [84, 124]

$$e, a, b, ab, ba, bab, \tag{C.5}$$

where e is the identity, $a = e_2$, $b = e_3$, and in this representation the elements a and ab correspond to reflections across a triangle and rotations of $2\pi/3$ respectively. As such, the three conjugacy classes can be classified as [84, 124]

$$C_1 : e, \quad C_2 : ab, ba, \quad C_3 : a, b, bab, \tag{C.6}$$

now that the conjugacy classes are determined, the character table is determined by applying the orthogonality relationship between characters from Eq. C.3, yielding [84, 124]:

Conjugacy Class	Elements	χ_1	χ_1	χ_2
C_1	1	1	1	2
C_2	3	1	1	-1
C_3	2	1	-1	0

Table C.1: Character table for S_3.

For Physicists, what is most relevant is how to write products of vectors with various assignments under the non-Abelian group in a way that forms a trivial singlet. Explicitly determining these terms thus yields the relevant terms in a Lagrangian in the basis where the discrete symmetry is manifest (before it is broken by soft terms or spontaneously). In the following sections, a brief description of the group, character tables, and the multiplication rules are listed in addition to a few explicitly written examples of applications of these multiplication rules. rules and character tables.

C.4 A_4

The alternating group of four elements, or A_4, is the group made of all even permutations of the S_4 group and is of order 12 [84] and has three one-dimensional representations,

and one three-dimensional representation. Utilizing the properties outlined in previous sections, the character table and multiplication rules are worked out. For specific details see Ref. [84].

C.4.1 Character Table

Conjugacy Class	Elements	h	χ_1	$\chi_{1'}$	$\chi_{1''}$	χ_3
C_1	1	1	1	1	1	3
C_2	4	3	1	ω	ω^2	0
C_3	4	3	1	ω^2	ω	0
C_4	3	2	1	0	0	-1

Table C.2: Character table of A_4.

C.4.2 Multiplication Rules

The multiplication rules for A_4 are

$$\mathbf{3} \times \mathbf{3} = \mathbf{1} + \mathbf{1}' + \mathbf{1}'' + \mathbf{3}_1 + \mathbf{3}_2, \tag{C.7}$$

which can be written explicitly given $\mathbf{A} = (A_1, A_2, A_3) \sim \mathbf{3}$, and $\mathbf{B} = (B_1, B_2, B_3) \sim \mathbf{3}$:

$$\mathbf{1} : A_1B_1 + A_2B_2 + A_3B_3 \tag{C.8}$$

$$\mathbf{1}' : A_1B_1 + \omega A_2B_2 + \omega^2 A_3B_3 \tag{C.9}$$

$$\mathbf{1}'' : A_1B_1 + \omega^2 A_2B_2 + \omega A_3B_3 \tag{C.10}$$

$$\mathbf{3}_1 : \begin{pmatrix} A_2B_3 + A_3B_2 \\ A_3B_1 + B_3A_1 \\ A_1B_2 + B_1A_2 \end{pmatrix} \tag{C.11}$$

$$\mathbf{3}_2 : \begin{pmatrix} A_2B_3 - A_3B_2 \\ A_3B_1 - B_3A_1 \\ A_1B_2 - B_1A_2 \end{pmatrix} \tag{C.12}$$

$$\tag{C.13}$$

C.5 D_7

The dihedral group of seven elements, or D_7, is the symmetry of a heptagon [2,79] which is the seven sided regular polygon (see Ref. [84] for more general dihedral groups) and it has two one-dimensional representations, and three two-dimensional representations.

C.5.1 Character Table

The character table for D_7 is:

Conjugacy Class	Elements	h	χ_1	$\chi_{1'}$	χ_{2_1}	χ_{2_2}	χ_{2_3}
C_1	1	1	1	1	2	2	2
C_2	7	2	-1	1	0	0	0
C_3	2	7	1	1	a_1	a_2	a_3
C_4	2	7	1	1	a_2	a_3	a_1
C_5	2	7	1	1	a_3	a_1	a_2

Table C.3: Character Table for D_7.

C.5.2 Multiplication Rules

The multiplication rules for D_7 are:

$$\mathbf{1}' \times \mathbf{1}' = 1 \tag{C.14}$$

$$\mathbf{1}' \times \mathbf{2}_i = \mathbf{2}_i \tag{C.15}$$

$$\mathbf{2}_i \times \mathbf{2}_i = \mathbf{1} + \mathbf{1}' + \mathbf{2}_{i+1} \tag{C.16}$$

$$\mathbf{2}_i \times \mathbf{2}_{i+1} = \mathbf{2}_i + \mathbf{2}_{i+2}. \tag{C.17}$$

These can be written explicitly given $\mathbf{A} = (A_1, A_2) \sim \mathbf{2}_1$, and $\mathbf{B} = (B_1, B_2) \sim \mathbf{2}_1$:

$$\mathbf{1} : A_1 B_2 + A_2 B_1 \tag{C.18}$$

$$\mathbf{1}' : A_1 B_2 - A_2 B_1 \tag{C.19}$$

$$\mathbf{2}_2 : \begin{pmatrix} A_1 B_1 \\ A_2 B_2 \end{pmatrix}, \tag{C.20}$$

and given $\mathbf{C} = (C_1, C_2) \sim \mathbf{2}_2$ then $\mathbf{A} \times \mathbf{C}$ yields

$$\mathbf{2}_1 : \begin{pmatrix} A_2 C_1 \\ A_1 C_2 \end{pmatrix} \tag{C.21}$$

$$\mathbf{2}_3 : \begin{pmatrix} A_2 C_2 \\ A_1 C_1 \end{pmatrix}. \tag{C.22}$$

C.6 $\Delta(27)$

The $\Delta(27)$ group is a dihedral-like group of $\Delta(3n^2)$ for $n = 3$, and has nine one-dimensional representations, and two three-dimensional representations. The character table, multiplication rules, and some relevant invariants are shown below.

C.6.1 Character Table

The character table for $\Delta(27)$, following the notation in Ref. [67] is:

Class	Elements	h	χ_{1_1}	χ_{1_2}	χ_{1_3}	χ_{1_4}	χ_{1_5}	χ_{1_6}	χ_{1_7}	χ_{1_8}	χ_{1_9}	χ_3	$\chi_{\bar{3}}$
C_1	1	1	1	1	1	1	1	1	1	1	1	3	3
C_2	1	3	1	1	1	1	1	1	1	1	1	3ω	$3\omega^2$
C_3	1	3	1	1	1	1	1	1	1	1	1	$3\omega^2$	3ω
C_4	3	3	1	ω	ω^2	1	ω^2	ω	1	ω	ω^2	0	0
C_5	3	3	1	ω^2	ω	1	ω	ω^2	1	ω^2	ω	0	0
C_6	3	3	1	1	1	ω^2	ω^2	ω^2	ω	ω	ω	0	0
C_7	3	3	1	ω	ω^2	ω^2	ω	1	ω	ω^2	1	0	0
C_8	3	3	1	ω^2	ω	ω^2	1	ω	ω	1	ω^2	0	0
C_9	3	3	1	1	1	ω	ω	ω	ω^2	ω^2	ω^2	0	0
C_{10}	3	3	1	ω^2	ω	ω	ω^2	1	ω^2	ω	1	0	0
C_{11}	3	3	1	ω	ω^2	ω	1	ω^2	ω^2	1	ω	0	0

Table C.4: Character Table for $\Delta(27)$.

C.6.2 Multiplication Rules

The multiplication rules for $\Delta(27)$ are

$$\mathbf{3} \times \mathbf{3} = \bar{\mathbf{3}}_1 + \bar{\mathbf{3}}_2 + \bar{\mathbf{3}}_3 \tag{C.23}$$

$$\bar{\mathbf{3}} \times \bar{\mathbf{3}} = \mathbf{3}_1 + \mathbf{3}_2 + \mathbf{3}_3 \tag{C.24}$$

$$\mathbf{3} \times \bar{\mathbf{3}} = \sum_{i=1}^{9} \mathbf{1}_i, \tag{C.25}$$

For the nine one-dimensional representations the multiplication rules are best labeled as in Table C.5 which allows the rules to be written as

$\mathbf{1}_i$	$\mathbf{1}_1$	$\mathbf{1}_2$	$\mathbf{1}_3$	$\mathbf{1}_4$	$\mathbf{1}_5$	$\mathbf{1}_6$	$\mathbf{1}_7$	$\mathbf{1}_8$	$\mathbf{1}_9$
$\mathbf{1}_{n,m}$:	$\mathbf{1}_{0,0}$	$\mathbf{1}_{1,0}$	$\mathbf{1}_{2,0}$	$\mathbf{1}_{0,1}$	$\mathbf{1}_{1,1}$	$\mathbf{1}_{2,1}$	$\mathbf{1}_{0,2}$	$\mathbf{1}_{1,2}$	$\mathbf{1}_{2,2}$

Table C.5: Alternative notation for $\Delta(27)$ singlets.

$$\mathbf{1}_{i,j} \times \mathbf{1}_{k,l} = \mathbf{1}_{i+k,j+l}. \tag{C.26}$$

The invariants in Eqs. C.23 and C.25 can be written explicitly given $\mathbf{A} = (A_1, A_2, A_3) \sim \mathbf{3}$, $\mathbf{B} = (B_1, B_2, B_3) \sim \mathbf{3}$, and $\mathbf{C} = (C_1, C_2, C_3) \sim \mathbf{3}$ (see Ref. [127] for more general discussion):

$$\mathbf{3}_1 : \begin{pmatrix} A_1B_1 \\ A_2B_2 \\ A_3B_3 \end{pmatrix} \tag{C.27}$$

$$\mathbf{3}_2 : \begin{pmatrix} A_3B_1 \\ A_1B_2 \\ A_2B_3 \end{pmatrix} \tag{C.28}$$

$$\mathbf{3}_3 : \begin{pmatrix} A_1B_3 \\ A_2B_1 \\ A_3B_2 \end{pmatrix} \tag{C.29}$$

$$\mathbf{1}_1 : A_1B_1C_1 + A_2B_2C_2 + A_3B_3C_3 \tag{C.30}$$

$$A_3B_1C_2 + A_1B_2C_3 + A_2B_3C_1 \tag{C.31}$$

$$A_1B_3C_2 + A_2B_1C_3 + A_3B_2C_1 \tag{C.32}$$

However, it is possible to make singlet combinations that are symmetric and anti-symmetric using Eq. C.31 and Eq. C.32 which take the form of

$$A_3B_1C_2 + A_1B_2C_3 + A_2B_3C_1 \pm (A_1B_3C_2 + A_2B_1C_3 + A_3B_2C_1), \tag{C.33}$$

writing this in the notation used in Ref. [67] this becomes

$$123 + 231 + 312 \pm (213 + 321 + 132). \tag{C.34}$$

The invariance under $\Delta(27)$ is easily checked by writing one of the elements of $\Delta(27)$ explicitly in a 3-dimensional representation and determining how a general $\mathbf{A}$ transform. For a specific choice for the 3-dimensional representation of an element of $\Delta(27)$ (see Refs. [84, 127] for some examples) then under $\Delta(27)$ the elements of $\mathbf{A}$ map $A_1 \to A_2$, $A_2 \to A_3$, $A_3 \to A_1$ and it is trivially demonstrated that Eq. C.33 is indeed invariant under $\Delta(27)$.